A Scalable 3D Printed Microfluidic Device for Rapid Preclinical Assays of Cancer Samples

By

Alex Markoski

B.S., Worcester Polytechnic Institute, 2018

Thesis

Submitted in partial fulfillment of the requirements for the
Degree of Master of Science in Biomedical Engineering at Brown University

PROVIDENCE, RHODE ISLAND

MAY 2020

This thesis by Alex Markoski is accepted in its present form by
the Center of Biomedical Engineering as satisfying the
thesis requirements for the degree of Masters of Science.

Date 4/27/2020

Ian Y. Wong, Advisor

Date 4/29/2020

Jeffrey T. Borenstein, Advisor

Recommended to the Graduate Council

Date 4/28/2020

Jeffrey R. Morgan, Reader

Date 4/28/2020

Jonathan Reichner

Digitally signed by Jonathan Reichner
DN: cn=Jonathan Reichner, email=reichner@brown.edu, c=US
Date: 2020.04.28 09:29:11 -04'00'

Jonathan S. Reichner, Reader

Approved by the Graduate Council

Date 4/30/2020

Marissa Gray (Apr 30, 2020)

Dr. Marissa Gray, Biomedical Engineering
Master's Program Director

Acknowledgements

The creation of this thesis and the work behind it could not have happened without the help and support of so many important people.

I want to give a special thanks to my advisor at Draper, Jeff Borenstein, for his guidance and positive outlook. Ever since I started at Draper, he has been an advocate for me and I look forward to more discussions on music in the future. I also wanted to thank those at Draper who helped answer my questions and supported me, special call out to the Fellow Cave.

I also want to give another special thanks to my advisor at Brown, Ian Wong, for his deep insight and help keeping me grounded and on track with my lofty project goals. Both he and the Wong lab have helped make me feel welcome and part of the Brown community. Additionally, I want to thank Jeff Morgan and Jonathan Reichner for agreeing to support me as thesis committee members.

To my family, your unwavering confidence, love, and support in me are constant anchors in my life which have continued to give me the energy to climb taller mountains. I can't thank you enough.

To my friends, you guys are the best and know how to cheer me up even when I'm miles away or have too much to do. Although I'm not always around you guys keep the door open for me and I couldn't ask for anything more. Keep on being awesome and thanks for the support.

A special thank you to my love who helped me through the tough times in these two years and supported me regardless of how much was on our plates or how far apart we were.

This work was sponsored in part by The Charles Stark Draper Laboratory, Inc.

Table of Contents

Table of Figures

List of Tables

List of Acronyms

ALI (Air-liquid interface)

AM (Additive Manufacturing)

CAD (Computer Aided Design)

COC (Cyclic Olefin Copolymer)

CTCF (Corrected Total Cell Fluorescence)

EVIDENT (*Ex vivo* Immuno-oncology Dynamic Environment for Tumor Biopsies)

FDM (Fused Deposition Modelling)

FFF (Fused Filament Fabrication)

ICI (immune checkpoint inhibitors)

PDMS (Polydimethylsiloxane)

SLA (Stereolithography)

TAP (Tumor Analysis Platform)

Abstract

Immunotherapies such as immune checkpoint inhibitors (ICI) show great promise as more efficacious treatments for various cancers compared to current methods like chemotherapy. However, preclinical evaluation of immunotherapies typically relies on mouse models that have questionable relevance to human responses, or on *in vitro* culture methods that suffer from small sample sizes, limited cell viability, a lack of physiologically relevant stimuli such as flow, and an absence of tumor-immune cell interactions. To address these limitations with current models, a scalable 3D printed microfluidic device capable of capturing multicellular tumor spheroids and perfusing them to extend sample viability for long term testing was developed. Finite element modeling was used to optimize flow conditions and capture efficiency. Tumor spheroids were used to validate extended sample viability over three days compared to standard static culture. The resulting device created was capable of being printed and ready for use within an hour and a half with novel integrated connectors for scalability and ease of use. An array of 3D printed micro posts was able to capture and hold both tumor spheroids and tumor fragments in line with flow for perfusion over time. Ultimately, these microfluidic devices will enable researchers and clinicians alike to test various immunotherapies in a scalable, rapid, and *in vivo* relevant manner.

1 Introduction

Microfluidics have become a widely used technology within the field of *in vitro* diagnostics due to their unique ability to simulate *in vivo* like geometries and flow conditions. These platforms' defining features typically revolve around a channel or series of channels on the micro scale which are capable of effective fluid flow. Methods utilizing PDMS (polydimethylsiloxane) or heated presses to imprint a channel geometry on a moldable polymer are common for the creation of microfluidics devices of varying complexity [1, 2, 3]. However, many microfluidic platforms are made using single layer replicas of photolithography master molds which require multiple steps to create. This process results in long fabrication times and a large financial investment put into a single device. This inhibits rapid testing and puts a heavy reliance on the manufacturing process to produce a perfect device each time. Additionally, many microfluidics are employed in the dynamic field of research which can sometimes move faster than the manufacturing process, in turn possibly invalidating a device in the manufacturing pipeline. In order to match the fast pace of research, the manufacturing process of microfluidic platforms must be able to match the rate of design iteration. Recent advancements in 3D printing technology have now been able to fill the need for a rapid low-cost manufacturing platform for microfluidics [3]. This is a relatively new and unexplored field and the manufacturing method used for the microfluidic device discussed in this thesis.

Microfluidic devices have become an effective platform for *in vitro* cancer modeling in the medical field. Traditionally, *in vitro* diagnostics have been dominated by static culture devices such as the simple 96 well plates which lack important *in vivo* stimuli like fluid flow. *In vitro* diagnostics have been moving towards incorporating more *in vivo* like signals since the closer the platform comes to mimicking a biological system the more *in vivo* like responses will

be received from the platform. This trend is extremely important to the field of biomedical engineering since the current gold standard for bringing a therapeutic to market or analyzing a biological situation is time consuming and resource intensive. Animal studies and static culture testing have been proven to be poorly predictive of how a therapeutic works in a human system. For example, 2D cell culture of cancer cells are much less resistant to chemotherapeutics than cancer cells found in the body due to the lack of cell-cell interactions and mechanical stimuli [4, 5]. Microfluidics provide more accurate results to *in vivo* by incorporating important stimuli missing from static environments.

There are a wide variety of microfluidic applications within the medical field from organ-on-a-chip systems to single cell analysis platforms, however one of the most impactful applications is within the field of cancer research as an *in vitro* platform [1]. Cancer is one of the leading causes of death in the US, attributing to every 1 in 4 deaths in 2014 with 1.5 million new cases annually as of 2016 [4, 6]. Microfluidic devices are helping test new cancer therapeutics and better understand the mechanics of the disease through metastasis models. One area of cancer therapeutics which has a need for a microfluidic model to supersede the traditional 2D static culture methods is the field of immunotherapies [2, 3]. Immunotherapies focus on empowering the body's own immune system to help target and fight an individual's cancer. These therapies can act as a means of personalized medicine where each treatment is partly constructed with the patient's own immune cells. However, despite the promise of this means of treatment, progress in this field has been slow and has had issues with adverse reactions due to the poor predictive power of preclinical animal models [2, 7]. Microfluidics could provide these therapies with a more accurate way to match a patient's treatment with their specific cancer via

the ability to provide an *in vivo* like environment which promotes immune cell-tumor cell interactions.

This thesis outlines the production of a novel scalable 3D printed microfluidic device for the purpose of capturing and rapidly analyzing the viability of cancer samples under flow conditions compared to traditional static methods. First, the methods of fabrication via the 3D printer were optimized to meet the desired feature resolution and imaging clarity as explained in section 3.1. The reasoning and iterations behind the major features in the final device design are explained in section 3.2. Device setup and sample preparation of both cancer spheroids and tumor fragments are outlined in sections 4.1, 4.2, and 4.3 respectively. Sections 4.4, 4.5, and 4.6 focus on the evaluation and results of the device's ability to capture samples effectively and sustain their viability over an extended duration compared to static culture. Section 5 concludes and summarizes the major findings from this thesis. Section 6 elaborates on possible future work stemming from the findings in the thesis.

2 Background

2.1 Methods of Microfluidic Fabrication

Microfluidic devices originated from manufacturing techniques developed by the semi-conductor industry. One of these major techniques is the process of photolithography which utilizes a multistep wash of chemicals and UV light to produce micron scale electronic features. This was later translated to be used in producing microfluidic features. Today, microfluidics have seen many advances from their inception in the late ‘90s in both applications and methods of manufacturing. Early microfluidics were used in a variety of applications from inkjet printing to miniaturized gas chromatography, it was not until later that they adapted new complex materials to support biological samples [8].

The draw to microfluidics for biological applications is derived from the scale and design flexibility to produce *in vivo* like geometries and channels. Additionally, the reduction in size often results in a reduction of needed resources such as the cell media required for experimentation. Micron scale features and channels opened up the potential for the addition of mechanical and flow-based stimuli including but not limited to shear stress, tension, and compression forces. Each of these aspects provided microfluidics with an advantage over typical static culture methods since these aspects allowed microfluidics to better match *in vivo* conditions. Static culture is still the baseline standard for many applications but the rise of complex microfluidic systems allowed microfluidics to become a more favorable option [8].

Some of the most prevalent fabrication methods used today for microfluidic devices include soft lithography, micro injection molding, and more recently 3D printing [8, 9]. Other options for fabrication include micromachining which is usually reserved for the production of

finalized designs of a limited number of replicates. Each of these options have advantages and disadvantages associated with their fabrication process and fulfill different requirements for a microfluidic device. However, to be usable for biological testing each process must produce a microfluidic device capable of effectively containing fluid for the duration of testing and produce microscale geometries [3, 8].

2.1.1 Soft Lithography and Embossing Lithography

Soft lithography is one of the most common modalities of microfluidic production centered around a combination of photolithography created molds and soft polymers. The first step of the fabrication process is to create a master mold with the desired microfluidic geometry. This is done via photolithography which etches the design on to the mold material via UV light reacting with a photoresist material. The result is a master mold with high feature resolution ready for molding. The second major component of this process is a soft polymer. Typically, PDMS is used to imprint the design by curing the pre-polymer solution on the mold and removing the cured construct. The resulting negative PDMS mold is then permanently bonded to a glass slide or other optically clear polymer and prepped for use. Overall, this process is fairly simple and allows for multiple devices of the same design to be created with relative ease. The creation of the pre-polymer PDMS requires very few steps and is a relatively inexpensive material. The master mold can be used multiple times if kept clean [9, 10].

There are a number of drawbacks to this methodology including the high initial cost and long time required to acquire and produce a master mold. There are alternatives to using photolithography to create a master mold such as laser cutting and machining the geometry but both options are typically at the expense of feature resolution. Difficulty acquiring a master mold also limits the ability to freely iterate on a design since each revision would require the

production of a new master mold. Additionally, PDMS as a material has limitations with certain biological applications. Specifically, PDMS has been seen to adsorb proteins and is a highly oxygen permeable material both of which can introduce uncontrolled conditions during biological testing [3, 9].

A resolution to some of the issues surrounding soft lithography can be found in embossing lithography. This process is largely the same as soft lithography with the exception of the material used for the creation of the negative mold. Instead of PDMS, a polymer with a low glass transition temperature such as COC (cyclic olefin copolymer) is pressed into the master mold under pressure and at high temperature [2]. The combination of these factors allows the master mold to imprint the geometry on to the polymer which is then cooled and removed from the master to be bonded to a glass slide or other clean polymer [2, 8]. This process, however, still shares the same master mold related issues as soft lithography.

2.1.2 Micro Injection Molding

The process of micro injection molding is fairly straight forward and provides the highest throughput out of all the fabrication methods discussed. A thermoplastic is heated past its melting point and while in a molten form is deposited into a cooled master mold with the microfluidic geometry. The cooled master mold facilitates rapid cooling and solidification of the thermoplastic which is then removed from the mold and left to further cool. The master mold in this application is made in similar ways to that of soft lithography and therefore carries its resolution advantages and an increased cost and time disadvantage [3, 11]. This process produces devices extremely fast and can even be automated for commercial device fabrication. However due to the method of extruding molten material into a mold the geometry of the microfluidic

device is limited. Despite that restriction, micro injection molded microfluidics are viable for biological applications, e.g. a device used to determine blood type made of COC [8, 12].

2.1.3 3D printing

One of the newest methods to enter the field of microfluidics is 3D printing. Although its inception was in the ’80s, 3D printing did not reach the levels of resolution and material variability required for biomedical grade microfluidics until the past 5 years or so [8]. Compared to the other mentioned fabrication processes, 3D printing is the only additive manufacturing (AM) based process. Compared to a subtractive process such as photolithography which etches material away to produce a microfluidic geometry, AM adds material to produce a complete microfluidic device [3]. In addition to this distinction, 3D printing is also the most flexible of fabrication processes due to its rapid build time and lack of reliance on a master mold. Generally, 3D printing consists of precursor material which is altered to be cured into a computer-aided design (CAD) based build layer by layer. This allows designs to be created and altered in a CAD software and then printed with very little down time in between. Furthermore, the devices can be made without excess material or the extensive costs associated with master molds or outsourcing for fabrication [3, 8]. Despite the advantages, this fabrication process has not been largely explored for the purpose of microfluidic development which is partially due to the difficulties of meeting the desired feature resolution [8].

Within the domain of 3D printing, there are variations with differing properties and techniques, the most common being fused deposition modelling (FDM) also known as fused filament fabrication (FFF) [3, 8]. This method utilizes thermoplastic filament which is extruded out of a heated nozzle which translates across a build plate in a programed pattern to form the build. Unlike other 3D printing methods, this method has the widest variety of materials to

choose from partially since it is the widest used 3D printing method. FDM, more so than some other 3D printing methods has trouble producing microfluidic channels on a micron scale resolution. The issue is due to various reasons from the size of the extruded filament being larger than the channels of the device to the adhesion between layers being insufficiently watertight [13]. The layers created by FDM produced devices are often visible and result in a non-transparent material finish which often limits the imaging capabilities for cellular based testing.

A more promising variation of 3D printing is stereolithography (SLA) printing. This process utilizes a resin bath to provide the material instead of an extrusion-based method like FDM. To produce a device, a vat of photoresin material is exposed to a focused laser or LED to cure the build layer-by-layer. The first layer to be printed is on the build platform which can either be in a free surface configuration or in a bat configuration. The free surface configuration, which is less common now, consisted of a plate being lowered into the vat of resin as the light source beams down from the top to cure each layer. More modern SLA printers utilize the bat configuration which consists of a hanging plate which drops down to the bottom of the bath where the light source beams up from the bottom curing each layer of the build. For both configurations, the build plate is lifted out of the vat after each layer is cured. Overall, the bat configuration provides builds with the best resolution and build size as it is not limited by the depth of the resin vat [13]. The amount of curing of the resin is dependent on the interactions between the 3D printer's light source wavelength and the resin's properties as well as the 3D printer's settings [13]. When optimized, this combination of factors can produce microfluidic devices of a high resolution with strong structural integrity. Post printing cleaning is required for these devices to clean channels of uncured resin. The major disadvantage of this method is that

the size of build plates can limit the total device size and there is usually a sufficient amount of optimization required to reach the desired parameters for printing [3].

Each microfluidic fabrication technique has advantages and disadvantages depending on the desired end product. However, SLA based 3D printing has seen significant recent advancements that make it the most favorable candidate for rapid iteration and flexibility associated with cancer research. Furthermore, it produces devices at the resolution and transparency required for cell-based analysis.

2.2 Methods of Evaluating Cancer Treatments

Cancer is a construction of mutated host cells that rapidly proliferate while evading the defensive measures of a host's own immune system. As a result of this disarming of the immune system, cancers can grow unrestricted into tumors. If these tumors are left untreated, they can spread cancer throughout the body via a process known as metastasis which can possibly lead to host death. Due to these attributes of cancer, it is paramount that the right treatment is found for treating an individual's cancer as quickly as possible to prevent tumor growth and metastasis. To further emphasize this point it was recorded in 2018 that cancer was the 2nd leading cause of death globally [14].

Currently, if a patient is diagnosed with a cancer their treatment is determined by the type of cancer, size, and the infected location in the body. Based on that information, a combination or single treatment of chemotherapy, radiation, surgery, and or immunotherapy is chosen for that patient. While this process has seen some measure of success, this methodology ignores the uniqueness of each patient's case. This impersonal approach to treatment is partially based on the lack of platforms capable analyzing a patient's cancer in a short amount of time. In order to personalize a patient's treatment, a genetic evaluation must be performed to analyze the patient's

specific type of cancer and match that to the genetic profile of others to determine a successful treatment plan [15]. This process can be lengthy, applicable to only a fraction of patients, and for some patients time is of the essence, therefore there is a clinical need for a fast way to assess which treatment or treatments is ideal for a specific patient without extensive genetic testing. Microfluidic devices and other cellular platforms have begun to fill in the need for assessing cancer rapidly. Examples of this include the TAP and EVIDENT systems both of which are capable of capturing cancer tumor fragments *ex vivo* and exposing them to immunotherapy treatments [2, 3]. Both of these platforms are designed to utilize tumor fragments which would be obtained from a patient's tumor biopsy in clinic for evaluation in their respective platforms. Post-acquisition, these samples are fragmented, stained for visualization, injected into the devices with flow to guide them into a capture geometry where the samples are held in place while further flow delivers various immunotherapies.

The TAP (Tumor Analysis Platform) is a 3D printed microfluidic device capable of capturing tumor fragments in its unique pocket capture geometry. This device is composed of a biocompatible resin matched with a high-resolution SLA 3D printer. The design of the TAP system is comprised of a threaded inlet, a bubble trap, pocket capture geometry, and a threaded outlet as seen in Figure 1. Additionally, the device, after post printing cleaning and polishing, is exceptionally translucent for cellular imaging. As mentioned previously, SLA based 3D printing is fast and allows for rapid iteration without sacrificing build integrity or feature resolution. For these reasons the TAP system is a strong candidate for rapid assessment of immunotherapies effect on a patient's cancer. Some of the drawbacks to this platform revolve around its large size and capture geometry. With respect to many other microfluidic devices the TAP is much smaller, however it has less channels per amount of size the device takes up. For this reason, the TAP is

not as easy to scale up for large scale testing. The capture geometry is mainly suited for large tumor fragments which could also limit its use with early stage cancers or cancers which have tumors that cannot be safely resected [3].

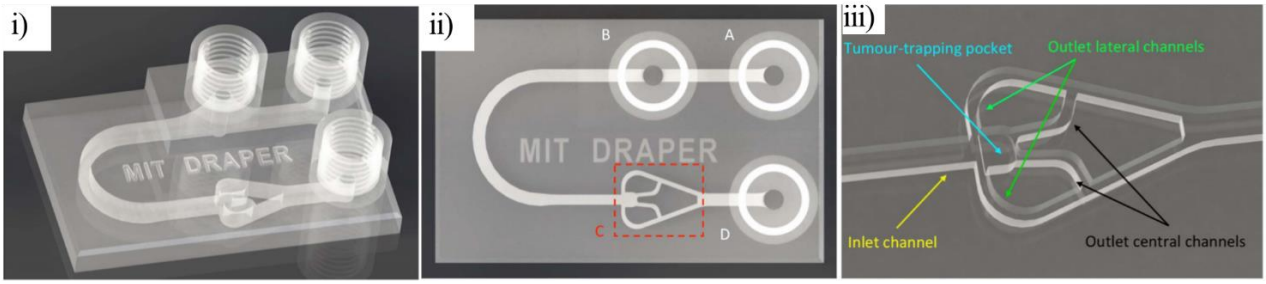

Figure 1. Multiple views of the TAP device adapted from [3]. i): Isometric view of the TAP device; ii): top down view of the TAP device and its major components with red box around the capture geometry; iii) labeled close up of the capture geometry.

The EVIDENT (*ex vivo* immuno-oncology dynamic environment for tumor biopsies) system is a COC based 12 channel microfluidic device designed for capturing small tumor fragments in its V-shaped post capture geometry. The device is created via a combination of embossing lithography and multilayer thermal bonding matched with external metallic ports epoxied into place post thermal bonding. The device is composed of 12 separate straight channels with two inlet ports (one for flow and the other for sample injection), a capture geometry consisting of five slotted posts, and an outlet as seen in Figure 2. The embossing lithography provides the EVIDENT system with extremely high feature resolution and having 12 channels allows for a higher number of replicates per test. The use of COC covered by another thin clear polymer also provides superior imaging clarity compared to the unpolished products of 3D printing. It should be noted however, that the complete EVIDENT system setup is much more involved than that of the TAP system comprising of different types of tubing, a pressure driven pump, and an external bubble trap. The EVIDENT system is also limited by its fabrication process which requires multiple steps to produce a single workable device. The

combination of fabrication limitations with the complexity of the complete system restricts the scalability of the platform as a medium for in clinic assessment [2].

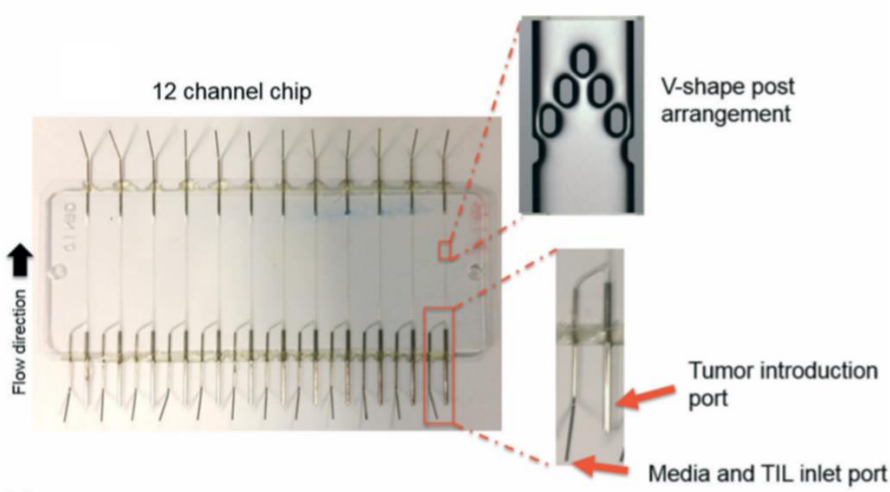

Figure 2. Top down view of the 12 channel EVIDENT device with close ups on the V-shaped post capture geometry and double inlets adapted from [2].

These devices both are steps in the right direction toward rapid assessment of a patient's cancer for personalized treatment, however neither of these are well suited for scaling up to the level required for clinical assessment. For the TAP system this limitation is the device's large capture geometry which is not suited for a wide variety of samples. For the EVIDENT system the limitation is built into the complexity of the complete system and its fabrication. Another limitation is around the biological medium of tumor fragments chosen by both platforms as a representative sample for testing. In clinic, a tumor biopsy would be the easiest medium to work with as it doesn't require any amount of excessive cell culture and is generally heterogenous in composition by nature. However, this heterogeneous nature in both its composition and size can provide complications for treatment assessment. Two other options for biological representation of a cancer tumor are tumor spheroids and tumor organoids which are explained more below. Both of these other options require external cell culture but can provide more replicates for testing over time compared to reliance on multiple biopsies needing to be taken from the patient.

Spheroids are typically an agglomeration of a single type of cells into the form of a sphere on the scale of 100µm to 500µm in diameter [16]. These spheres of cells are formed by leveraging a cell's ability to produce cell to cell interactions to create a 3D construct. There are multiple ways of achieving the result of a spheroid but two of the most common methods are the hanging drop technique and the use of non-cell adherent surfaces. Both of these methods are forms of static culture. The hanging drop technique consists of seeding cells into droplets of media which are then hung upside down. The cells are then forced to agglomerate at the bottom of the droplet in turn forming a spheroid over the course of 24 to 48 hours [17]. This process is not very resource intensive but is very low throughput and sensitive as any wrong movement could dislodge the droplets [18]. Use of non-cell adherent surfaces is an easier and higher throughput option for spheroid production. This consists of seeding cells into molds or wells composed of a non-adherent material such as agarose or a nonadherent cell culture dish. Without a material to latch on to the cells are prompted to form cell-cell connections in turn producing a spheroid. Platforms such as 96 well plates or Microtissues's 3D Petri Dishes are capable of producing spheroids of varying diameters in a high throughput manner for large scale testing within the span of 24 to 48 hours post seeding of the cells [18, 19]. One of the major advantages of spheroids is the uniformity in size and composition. This allows for a more equal distribution of a treatment when captured in a device and helps to reduce the variability between samples allowing for more conclusive results. The downside to spheroids is the requirement of cell culture to produce enough cells for spheroid formation as well as their lack of heterogeneity [3]. Additionally, not every cell type is effective in forming spheroids. The size of spheroids is often limited to less than 500µm in diameter due to diffusion limits which restrict essential nutrients from reaching all the way to the core of the spheroid. The result of this limitation is the

formation of a necrotic core from hypoxia related cell death which can negatively impact data acquisition [5]. While having less variability in composition can be beneficial towards specialized testing, having a format that is more equally representative of a complete tumor is closer to *in vivo* conditions.

Organoids are the next level of complexity past spheroids for cell culture. These biological constructs are cultured from multiple cell types from a patient's tumor sample to form effectively an *ex vivo* tumor. This can be done through multiple approaches, two of the most common for producing patient specific organoids are culturing a patient biopsy in an air-liquid interface (ALI) system and breaking down the fragment via enzymolysis and growing the cells in a 3D microenvironment. ALI culture utilizes a special insert for a well plate which is coated with a 3D biological matrix such as Matrigel. The tumor biopsy is fragmented and seeded into the Matrigel which is hanging above a well with the appropriate media for the cell type. Over time this combination produces organoids which can be harvested from this system and prepared for use [20]. This process is capable of producing organoids which are so similar to *in vivo* that they are capable of surviving 44 days in native tumor microenvironments [20, 21]. The process of enzymolysis and 3D culture is similar to ALI except it chemically breaks down the tumor fragment into individual populations of cells which are then seeded into a 3D microenvironment for culture. Both of these processes take 4 to 12 weeks to fully create organoids from a patient's sample [21]. While organoids are the closest to matching *in vivo* tumors, they are the most resource intensive method with the longest time of production for samples.

A way to think of each biological medium is as if you are taking a figurative picture of the composition of a patient's cancer as depicted in Figure 3. A tumor fragment provides only

part of the picture, a tumor spheroid is a clear but zoomed in picture, while an organoid is similar to a polaroid which can take a large picture but requires time to produce.

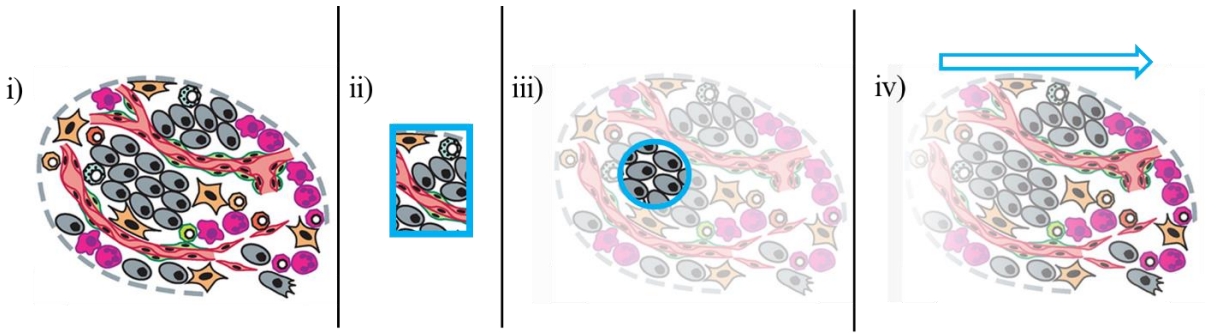

Figure 3. Depiction of figurative method for understanding biological mediums adapted from [22]. i): A heterogenous tumor composition; ii): a boxed snapshot of the complete tumor representing a tumor fragment; iii): a focused view of a specific cell type of the tumor representing a spheroid; iv): a practically transparent polaroid like view of the tumor representing an organoid.

For the purpose of rapid cancer analysis, tumor fragments and spheroids are more feasible than organoids despite their superior similarity to a complete tumor. While tumor fragments are more heterogenous than spheroids they can sometimes provide inaccurate results due to their variability in shape and composition, especially when used with a treatment assessment platform such as TAP or EVIDENT. Spheroids seem to be the happy medium between fragments and organoids for a consistent and quick assessment of a given cancer treatment.

3 Platform Development

3.1 3D Printing Optimization

The 3D printer used for development of all platform designs was the Asiga Max X27 (Asiga, Sidney, Australia), which was chosen for its superior dimensional accuracy and ability to print features on a micron scale. Specifically, this SLA based 3D printer has a pixel size of 27µm by 27µm allowing for the production of very small features in the microfluidic platform. The Asiga Max X27 is also compatible with a number of biocompatible resins such as Pro3dure GR-1 (Pro3dure Medical GmbH, Dortmund, Germany) which was chosen for its biocompatibility over extended periods of time [3]. This resin also is compatible with the Asiga's light wavelength of 385nm.

Despite these compatibilities, optimization of the 3D printer settings was required to create features on a sub 100 micron scale since there no presets made for the Pro3dure resin. The primary factors assessed for optimization were layer thickness, cure through multiplier, and offset value. SLA printers develop builds by curing layer by layer and the layer thickness determines the height of each one of the layers. This factor inherently limits the size of build features to the size of the layer thickness. The cure through multiplier is defined as the cure thickness coefficient which is factored into the 3D printer's calculations when defining the over curing per layer. As the 3D printer cures each layer it also cures past the assigned layer thickness which helps ensure effective bonding between each layer. The offset value in conjunction with the multiplier determine the amount the printer cures into previous layers. An imbalance in these factors can cause underdeveloped features or clogged channels due to over curing per layer. Testing values for each of these factors were determined based off recommendations given from the manufacturer of the 3D printer, previous literature, and printer limitations. Layer thickness

values assessed were 10µm, 25µm, 50µm, and 100µm, cure through multipliers assessed were 0.1, 0.5, 1, and 2, and offset vales assessed were 10µm, 40µm, 60µm, 200µm, 272µm, 600µm.

A resolution testing platform was developed in SolidWorks 2016 (Dassault Systemes, Waltham MA, USA) to assess how these factors manifest themselves with respect to important design features for the device. Specifically, the resolution testing device focused on the channel and posts since these features required the highest resolution since they are the components which will be interacting with biological samples. Posts' diameters were evaluated in multiples of the 3D printer's pixel size increasing from 27µm to 270µm at two heights of 125µm and 250µm. Channel sizes for evaluation ranged from 650µm wide by 125µm high to 1mm by 1mm. Additionally, layer thickness was assessed via 10µm incremental stacked slots. A schematic of the final revision of the resolution testing device can be seen in Figure 4.

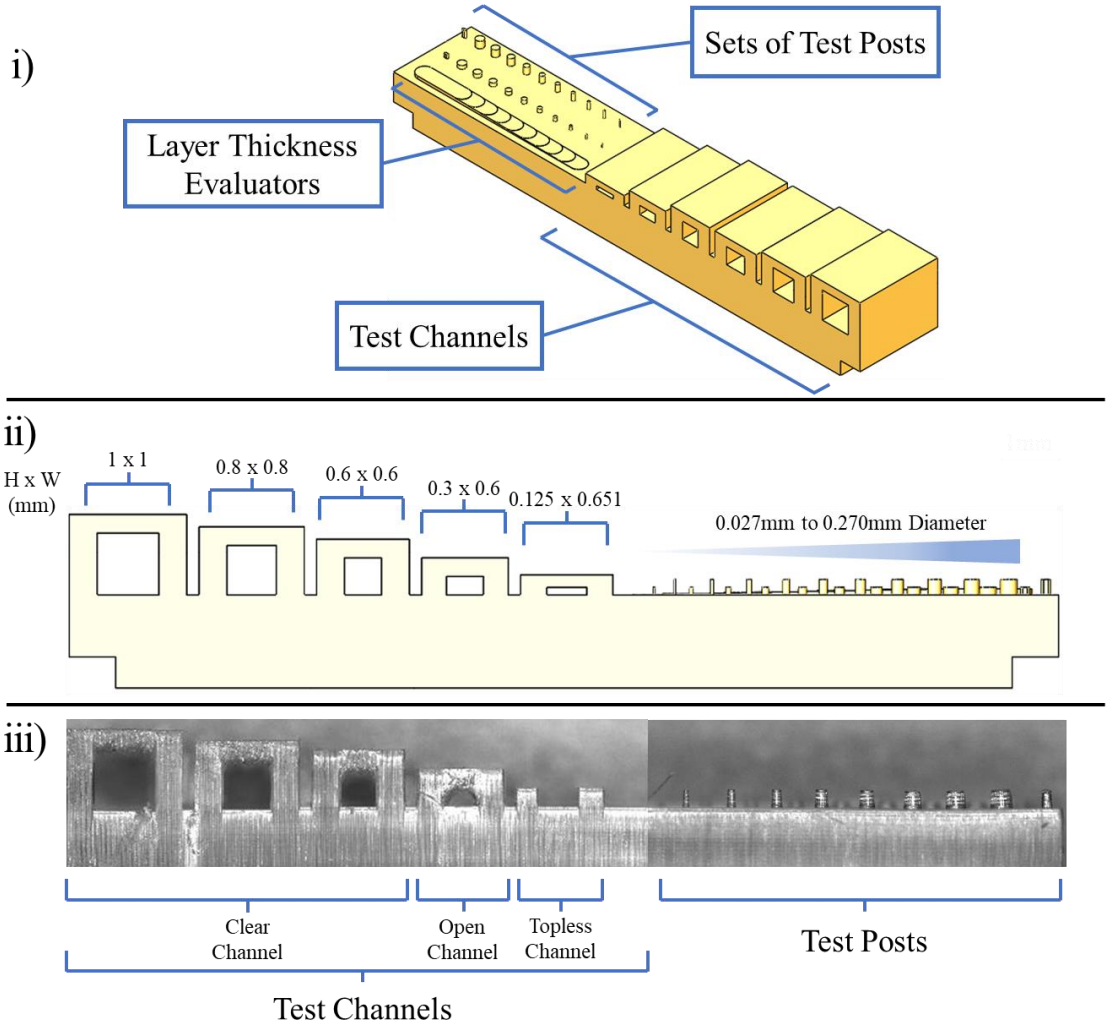

Figure 4. Views of resolution testing device. i): Isometric view of the Resolution Testing Device composed of three major components: Test Channels, Test Posts, and Layer Thickness Evaluators; ii): Side view of Resolution Testing Device highlighting expected channel size and posts; iii): Side view of a resolution testing device showing examples of clean, open, and topless channels.

Before printing each variation, a preview of the build layer by layer was produced by the Asiga Composer software which helped to rule out variations that had no chance of success. Based off these tests it was determined that a layer thickness of 50µm, cure through multiplier of 1, and an offset value of 272µm produced the best combination of posts and channels. Table 1 shows a culmination of the results collected for each variation with green colored cells to signify the best results while Appendix B1 shows a more detailed version. The primary metrics assessed

were the number of pillars formed, the number of open channels, the number of clean channels, and number of fully formed channels. Open channels were defined as channels which had an unblocked clearing from one opening of the channel to the other but was smaller or more uneven compared to the intended CAD file. Clean channels were channels which adhered closely to the CAD file's geometry and dimensions. The most common issues seen were channels being clogged with cured resin due to over curing, the tops of channels not printing, and pillars with a diameter of 81µm and below not staying on the platform during cleaning post printing. Examples of the test channel and test post classifications are depicted in Figure 4. A Keyence VR-3100 scanning white light interferometer (Keyence, Osaka, Japan) was used to image each resolution testing device and the VR-3000 Series Analyzer Software (Keyence, Osaka, Japan) was used to analyze each image. Once optimized, the feature resolution for the height and width of the channel when normalized with respect to the 3D CAD model showed a 2.1% (9.2±8.2µm) and 2.9% (22±10µm) difference respectively.

Table 1. Factors tested and associated results from the Resolution Testing Device normalized with respect to the CAD file. The best results are colored green to simplify evaluation. A Layer Thickness of 0.05, a Multiplier of 1, and an offset value of 0.272 provided the best results overall.

Factor Combinations Tested			Resolution Testing Device Results		
Slice Thickness (mm)	**Cure Through Multiplier**	**Offset Value**	**0.25mm Pillars Formed (%)**	**0.125mm Pillars Formed (%)**	**Clear Channel (%)**
0.01	1	0.1	50	50	75
0.01	1	0.01	0	40	0
0.025	1	0.1	0	0	0
0.05	1	0.1	0	0	0
0.05	1	0.2	80	80	40
0.05	1	0.272	80	80	83.3
0.05	0.5	0.272	80	80	60
0.05	2	0.272	90	90	0
0.05	0.1	0.272	80	80	60
0.1	1	0.1	70	80	25
0.1	1	0.04	60	70	25
0.1	1	0.6	90	90	0
0.1	1	0.06	70	80	50
0.1	1	0.01	60	70	25
0.1	1	0.2	80	80	60

3.2 Device Features

The design and features of the 3D printed device was influenced by the assessment of the pros and cons compared to other platforms such as EVIDENT, TAP, and static culture systems discussed in section 2.2 [2, 3]. With this in mind, the 3D printed device was designed with multiple features built into it for ease of use and set up. These features consist of a single channel with three threaded ports along the channel for the inlet, bubble removal, and outlet. Most importantly, there is a series of posts in a v-shaped formation between the bubble trap and outlet for the purpose of capturing tumor constructs for examination over time. Additionally, the external sides of the device have puzzle piece like connectors to maximize the flexibility and scalability of the device for any testing setups. Each device has been minimized to a size 46mm

by 16mm by 10.6mm while still integrating all critical components within a single monolithic platform. A complete schematic of the device can be seen in Figure 5.

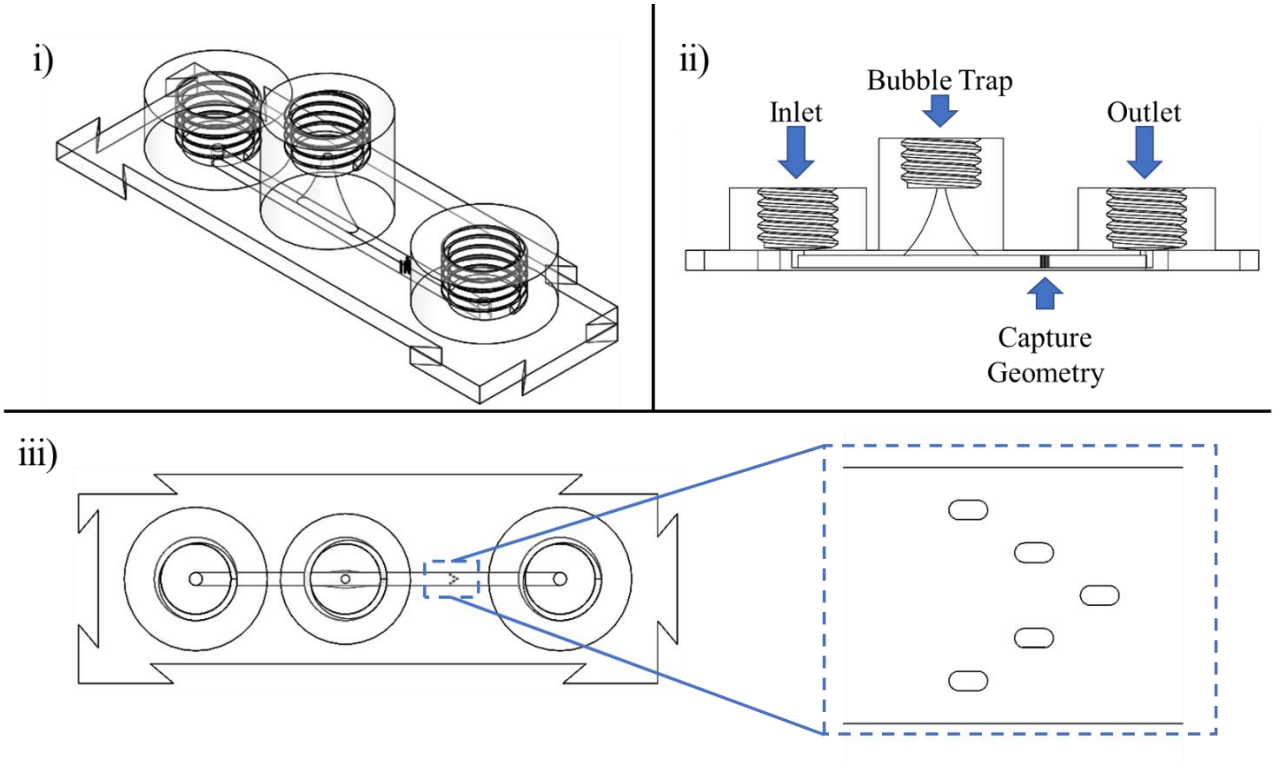

Figure 5. Multiple views of the developed device with annotations. i): Isometric view of the device; ii): cross-sectional view through the center of the device with labels for important feature; iii): top down view of the device with an expanded view of the capture geometry.

3.2.1 Channel

A single straight channel was chosen for its simplicity, modifiability, and flow characteristics. With a short straight channel, the tumor construct would have less chance of getting caught mid channel since the distance is minimized between where it is injected into the system and the capture geometry. Samples would be able to reach the capture geometry within 30 seconds of being injected into the channel and would settle in the capture geometry within minutes.

3.2.2 Bubble Trap

Microfluidics are often prone to bubbles getting caught within channels especially when changing tubing connections or injecting something into the system. At the micron scale bubbles can significantly impede flow or imaging and also harm the biology being examined [2, 3]. Once these bubbles enter the system, they are often very difficult to remove which is why having a component to help reduce the risk of these bubble reaching the capture geometry segment is beneficial. The bubble trap was designed to stop any bubbles from reaching the capture geometry by creating a tall curved chamber which allows bubbles to rise up and out of the path of flow which is located that the bottom of the chamber. As bubbles enter the device, the flow would direct them towards the bubble trap where, due to their buoyancy, they would follow the path of the top of the channel up and out of the path of the flow. The curvature of the chamber is such that it narrows in a parabolic manner towards a port at the top of the chamber which can be used to remove any trapped bubbles. Removal of bubbles is done by removing any connectors in the bubble trap and letting flow push the bubbles out the top of the port. This bubble trap is similar to ones seen in the EVIDENT and TAP systems, however the one implemented here is smaller and more compact in size [2, 3]. Having a port this close to the capture geometry also makes it a feasible option for tumor construct injection.

3.2.3 Capture Geometry

The capture geometry is the most crucial feature of this design since it serves the purpose of capturing a biological sample without damaging it throughout the testing process. This feature was iterated on multiple times to find a design which would ensure capture without occluding the channel, physically damaging the sample upon contact, or preventing flow and nutrients from reaching the sample. The choice of using a series of posts was derived from a combination of the

EVIDENT system's success, the limitations of the Asiga 3D printer, and its adaptability to a variety of sample sizes (200µm to 700µm). The capture geometry consists of a series of five slot shaped posts in a V-shaped formation which are oriented in line with the channel flow such that a biological sample will be captured and sit in place with the surrounding posts. A close up of this configuration can be seen in the furthest right channel in Figure 6.

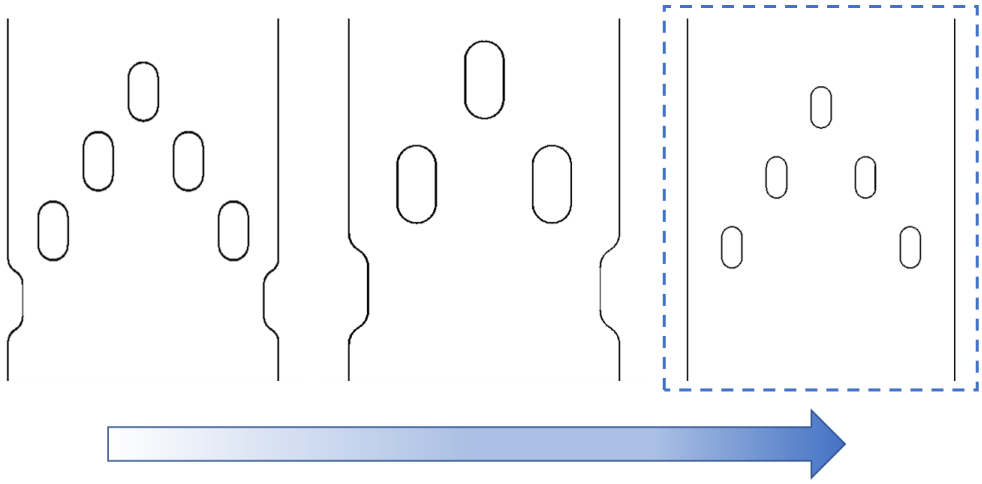

Figure 6. Example of the progression of revisions with the final channel geometry boxed on the far right.

Due to the posts configuration the sample is held in the center of the channel to promote effective perfusion of nutrients and exposure to physiologically relevant shear rates of 0.04Pa [3, 4, 23]. This was validated via a COMSOL simulation as seen in section 4.5 which helped to guide the revisions of the capture geometry. Furthermore, the posts were also designed to ensure effective capture while minimizing the amount of contact between the sample and surfaces of the posts such that flow was able to reach as much of the sample as possible. As long as flow is coming from the inlet to the outlet, the sample should stay in place but the design also allows for flow in the opposite direction for removal of the sample for further analysis post testing.

3.2.4 Connectors

An especially unique feature to this device is the connector geometry located around the perimeter of the device. The goal of these connectors is to allow for any number of configurations to be achieved with this device and in turn remove any restrictions to test sample size or setup. As long as these devices have a flat surface to rest on, they are able to connect to each other on each side without restriction as depicted in Figure 7. The connector geometry has a tolerance of around 200µm which allows for minimal resistance when linking devices while ensuring a tight connection.

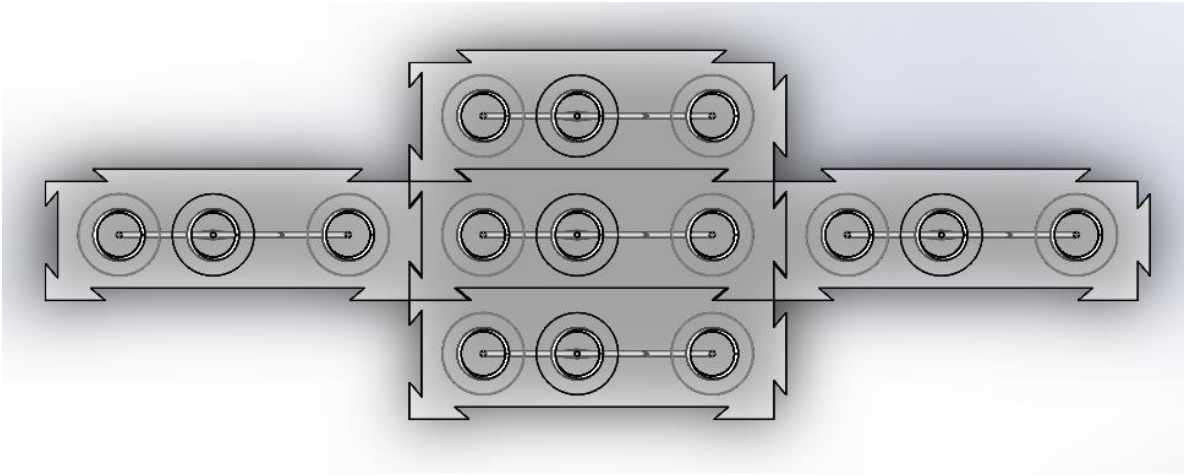

Figure 7. Top down view of 5 devices connected via interlocking the external geometry.

4 Evaluation of Platform

The purpose of this chapter is to outline the preparation of the system as well as the tests used to evaluate the device. Specifically, the tests outlined involve the use of CT26 tumor spheroids and human tumor fragments with the purpose of testing extended longevity compared to static culture. These tests also provided data on capture efficiency and interactions between the biological samples and the capture posts.

4.1 Device Preparation

To create one of these 3D printed devices, first the design was created in a CAD program such as SolidWorks. Once created the file was saved as an STL file type and changed to “Fine” to ensure the highest resolution. This file type is then imported into the Asiga’s custom software called Composer which allows the user to set the building parameters such as layer thickness as well as the builds orientation with respect to the 3D printer’s build platform. By connecting the computer to the 3D printer via an ethernet cable the build can be transferred for printing. Before each build, the resin bath was inspected to validate that the resin bath was filled to a height of 10mm and that there was no visible debris in the resin. Additionally, the LED function on the 3D printer was turned on for 10 seconds to create a cured rectangle which was used to remove any other debris before removing it from the bath. The build was then commenced and would finish the device in around 45 minutes. Using a specialized flat razor, the build was removed by shimmying the razor between it and the build platform while preparing to catch it with a free hand. Once removed the device was post treated by a three step cleaning procedure consisting of a 5 minute clean in a “dirty” bath of 97% isopropanol, a 5 minute clean in a “clean” bath of 97% isopropanol, and then drying with an air gun. The channel is further cleaned by running 97% isopropanol into the channel via a syringe connected to the outlet port. This procedure is required

to remove any remaining uncured resin which is not biocompatible and could clog up the channel if left over time. A multistep process described in a protocol in Appendix C1 was used to polish the device in the capture geometry region to improve imaging clarity and quality. 3600, 4000, and 6000 grit sandpaper was used sequentially to polish the capture region by moving the sandpaper in a circular motion at a constant pressure for one minute per grit level. This is required to remove the rough surface on the bottom surface of the device which was a result of being printed on the build platform which is not perfectly smooth to help builds adhere to the bat configuration build platform. A Taylor Hobson Form Talysurf PGI Freeform surface profilometer (Taylor Hobson, Berwyn, Pennsylvania, USA) was used to assess the average surface roughness of the polished area to optimize this protocol. Based on the profilometer data, this process was able to reduce the average surface roughness by 85% from an average surface roughness of 2.4±0.25µm before polishing to 0.35±0.06µm after polishing. A post cure in nitrogen gas for 3 minutes completely cures the device, readying it for use with biological samples. The complete protocol for device creating and post treatments is in Appendix C2. Overall, the process to produce a device ready for testing is under an hour and a half.

4.2 Platform Preparation

The built-in connectors of the device allow for a plethora of combinations depending on the desired test. In addition to these connections each device, regardless of configuration, has specific requirements for tubing, connectors, and flow. A simple configuration can be seen in Figure 8 which highlights the organization and ease of set up for the system.

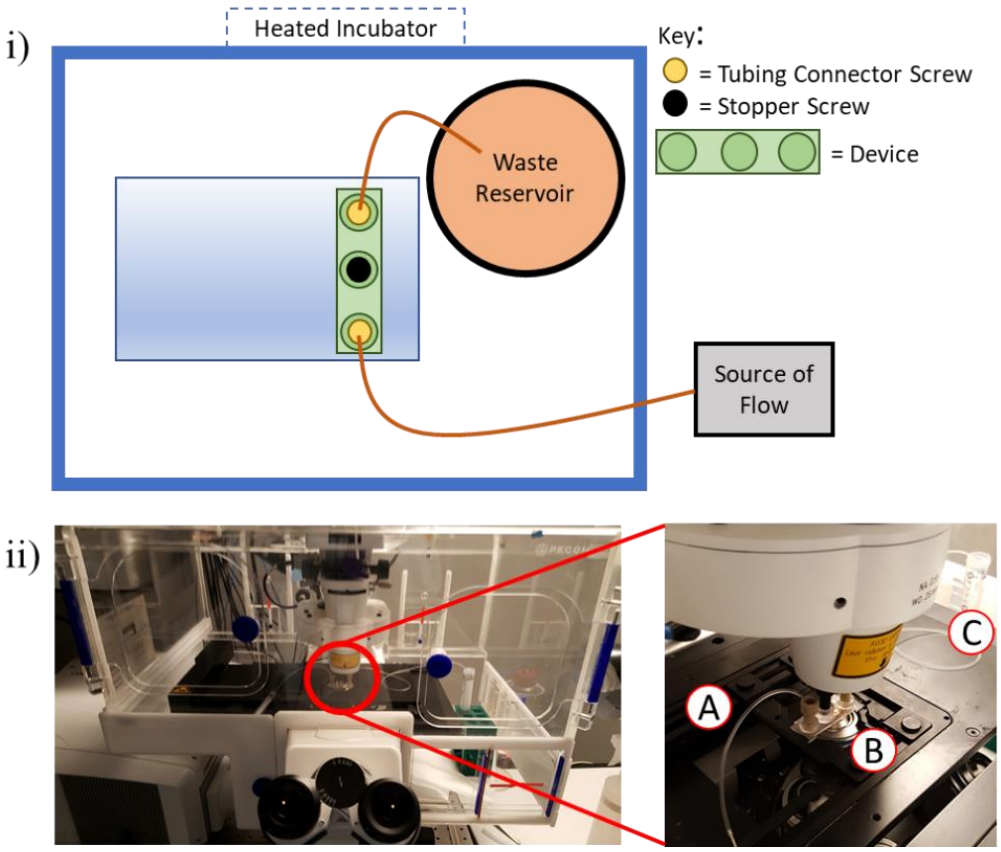

Figure 8. i): Top down schematic of a simple device configuration; ii): example of the schematic on a Zeiss LSM 710 confocal microscope with enhanced image showing, A) Source of Flow, B) Device, and C) Waste Reservoir.

The source of flow is ideally provided by a peristaltic pump allowing for continuous perfusion, however syringe pumps such as the Harvard Apparatus Standard Infuse/Withdraw PHD ULTRA™ Syringe Pump (Harvard Apparatus, Holliston, MA, USA) are also viable for limited duration testing. PFA tubing (1514L, IDEX Health Science LLC, Oak Harbor, WA, USA) is first connected to PEEK tubing connectors (XP-235X, IDEX Health Science LLC, Oak Harbor, WA, USA) which then are screwed into the inlet and outlet of each device. Each component was sterilized before set up based off their recommended technique which is listed in Table 2. Once connected, the bubble trap port is closed using a 1/4-28 Flat-Bottom Plug (P-309, IDEX Health Science LLC, Oak Harbor, WA, USA), leaving the system ready for priming and

testing. This set up was designed for use in an enclosed Zeiss LSM 710 confocal microscope (Zeiss, Oberkochen, Germany) for imaging of the samples.

Table 2. List of products and sterilization techniques used in conjunction with the device.

Product Name	Definition	Supplier	Catalogue #	Sterilization
Tubing	PFA Tubing Natural 1/16" OD x .030" ID	IDEX	1514L	Autoclave
Tubing Connector Screw	Flangeless Fitting Short, PEEK, 1/4-28 Flat-Bottom for 1/16" OD	IDEX	XP-235X	Autoclave
Syringe	20mL packaged	BD	309661	Sterile as packaged
Stopper Screw	Plug - Delrin®, 1/4-28 Flat-Bottom	IDEX	P-309	Autoclave
Syringe-Tubing Connector	Luer Lock hub with a 21 gauge blunt tip	Jenson Global	JG21-0.5HPX	Ethanol

4.3 Sample Preparation

The primary biological samples tested with this device were CT26 spheroids and human tumor fragments. These samples were chosen due to the morphological and composition-based differences which allowed for thorough evaluation of the capture efficiency and validation of the flexibility of the devices for use with various biological samples. Capture efficiency is defined as the ability of a device to capture a biological sample once introduced into the system. All cell culture work was executed with sterile techniques in biological hoods.

4.3.1 Spheroid Creation

The spheroids created for testing with the device were of a homogenous composition of CT26 cells which were capable of producing spheroids with diameters of 200µm to 500µm. CT26 cells acquired from ATCC are a colon carcinoma cell line which has been proven to create effective spheroids for immunotherapy based experiments [24]. As mentioned in section 2 larger spheroids have diffusion restrictions at larger diameters, therefore spheroids were evaluated between 200µm and 500µm to limit the development of a necrotic core. This restriction was also determined by the limitations of the capture geometry size which was not predicted to be able to reliably capture spheroids under 200µm. This determination was derived from the size of the spacing between the posts which would be large enough to allow for sub-200µm spheroids to pass through.

After acquisition from ATCC, the CT26 cells were placed in liquid nitrogen vapor phase storage until needed for spheroid creation. Once ready for use, the CT26 cells were removed from the liquid nitrogen tank and placed in a 37˚C water bath for about two minutes or until only a small frozen pellet remained in the vial. A 15mL centrifuge tube was filled with 4mL of RPMI-1640 complete medium which was formed via the combination of RPMI-1640 media and 10% FBS, fetal bovine serum, both acquired from ATCC. The contents of the CT26 vial were transferred to the 4mL of complete media and prepped for centrifuging. After centrifuging for five minutes at 300g, the supernatant was aspirated and the bolus of cells was resuspended in 1mL of complete medium. The CT26 cells were then transferred to a T25 flask prefilled with 8mL of complete medium and placed in an incubator at 37˚C and 5% CO2. The cells were closely monitored over the next day or two until the flask was visibly confluent at which point the cells were split at a ratio between 1:4 and 1:10 depending on when the cells were needed.

During the splitting, some of the remaining cells were transferred into cryogenic vials which contained about 1mL of freeze medium (95% complete growth medium, 5% DMSO) at a concentration of about five million cells per vial. Each vial was then labeled with date, cell type, number of cells per mL, and creator of the vial and then placed in a CoolCell Freezing System. The cells in the container spent three hours in a -20˚C freezer, overnight in a -80˚C freezer, and then the vials were individually placed in a liquid nitrogen tank for future use.

Creation of spheroids was facilitated via the use of Microtissues's 3D Petri Dishes [19]. These 3D Petri Dishes act as negative molds and when molten agarose is cured over them the result is an agarose mold with rounded wells. Agarose acts as a non-adhesive material for cells which in turn prompts cells to form cell-cell connections creating a spheroid. The cooled agarose molds were placed in a 12 well plate and prepared for the introduction of cells by soaking in 2.5mL complete growth media twice for 15 minutes. For production of 200µm diameter spheroids, 24-96 3D Petri Dishes were used and 24-35 3D Petri Dishes were used for 300µm and 500µm diameter spheroids [19]. Each mold also has associated cell counts recommended for effective seeding to reach each diameter, therefore the CT26s were counted to determine if the population size was sufficient for seeding. Before seeding each agarose mold, the CT26 cells were stained with CellTracker Green CMFDA Dye (Invitrogen C7025) at a concentration of 20µM in PBS for 15 minutes after being trypsinized using 1mL of a Trypsin EDTA solution. CellTracker Green freely diffuses into the cells and is changed into an irremovable fluorescent product allowing for easy imaging of living cells. The cells were stained before spheroid creation to eliminate any issues with diffusing the stain into the center of the spheroid. Once the CT26 cells were stained they were resuspended in complete media diluted to the required concentration for the desired spheroid size. The cells were introduced to 3D Petri Dishes drop-wise via a

pipette while moving the tip over the surface of the 3D Petri to distribute the cells evenly while removing the formation of bubbles in the wells. The CT26 cells were then left to form cell-cell connections over the course of 48 hours. Evaluation of spheroid creation and diameter was accomplished through visual inspection using a Zeiss LSM 710 confocal microscope. Figure 9 shows 200µm and 500µm CT26 spheroids in the 3D Petri Dish highlighted via the CellTracker Green fluorescence. Spheroids were removed from the 3D Petri Dish by inverting the 3D Petri Dish and centrifuging for 5 minutes at 500rpm. This process facilitates dislodgment from the agarose well, allowing for retrieval of the spheroids for introduction into the device.

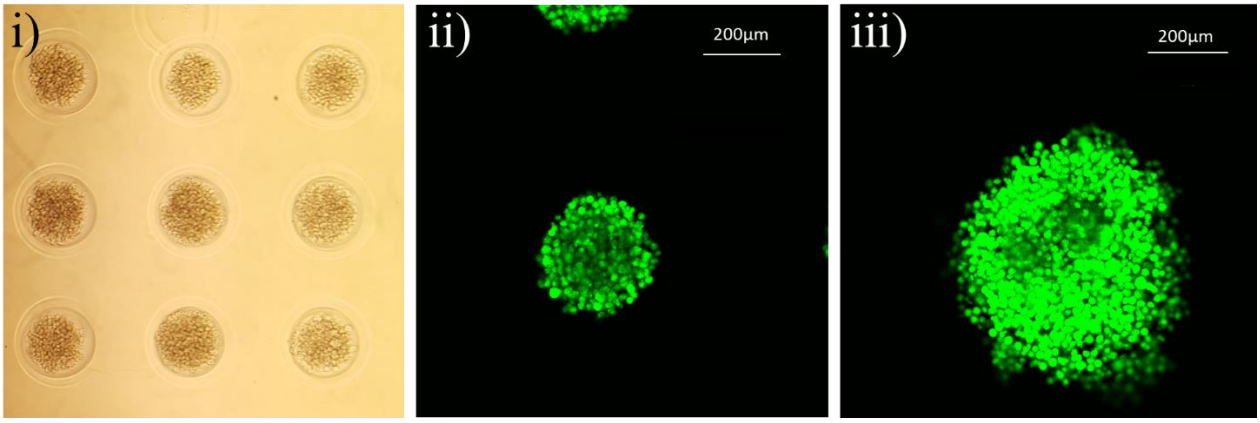

Figure 9. Images of CT26 spheroids in the 3D Petri Dish. i): CT26 cells forming spheroids in the agarose 3D Petri Dish; ii): 200µm spheroid in the agarose 3D Petri Dish; iii) 500µm spheroid in the agarose 3D Petri Dish.

4.3.2 Tumor Fragment Creation and Preparation

All tumor fragments tested were acquired from a clinical source and arrived as tumor samples around 1cm by 1cm in dimensions. The samples were from human carcinomas and were manually fragmented. Depending on the tumor sample's size and geometry, a biopsy punch was utilized to create tumor fragments around 700µm to 1000µm in diameter. Fragments from this method are then visually chosen and drawn into a syringe for injection into the device. A secondary method for fragmenting thicker tumor samples utilizes a combination of a syringe and

suction to tear pieces off the sample. A syringe is used to penetrate the surface of the tumor sample and once in the sample, the syringe plunger is drawn back to add suction to the sample which removing the syringe to create a small fragment. This method also produces fragments around 700µm to 1000µm in diameter but it also can produce smaller fragments around 400µm in diameter which are closer in size to the tested spheroids. Similarly to the spheroids, the chosen fragments are treated with CellTracker Green CMFDA Dye (Invitrogen C7025) at a concentration of 20µM in PBS except the fragments are exposed for 1 hour at 4˚C. The extended duration at a lower temperature allows for deeper diffusion of the CellTracker into the fragment while preserving the viability of the fragment over the duration of an hour. Post treatment, the fragments are observed under fluorescent microscopy to evaluate each fragment's viability indicated by green fluorescence. Only the fragments with the highest viability and proper sizes are chosen for implementation into the device for further testing [2, 3].

4.4 Loading of Samples and Capture Evaluation

Once the device was set up as depicted in the Platform Setup Section, a 5mL syringe with a gauge 12 blunt tip was used to obtain the biological samples for transfer into the device's bubble trap port. Alternatively, a pipette tip can be used to take in the sample depending on the size of samples used. The device was filled with complete media and the bubble trap port was vented to remove any bubbles. A stopper screw was also placed on the inlet after filling the device with media to prep for spheroid transfer. The 5mL syringe was partially filled (about 2mL) with complete media before attempting to remove the spheroids from the 12 well plate. The extra media was used to promote transfer of the sample into the device's channel. The injection was done slowly by hand by dipping the syringe into the 12 well plate and visually choosing a spheroid. As to not break apart the sample from excessive flow and shear rates, the

syringe was dipped into the well about 2mm from the sample and sucked into the syringe only until it was not visible. Removal of the syringe also must be done slowly and at an angle such that the syringe is parallel to the floor to prevent dislodgment of the spheroid from the tip of the syringe. Transfer into the channel was done by slightly pushing the syringe's plunger with the syringe inside the bubble trap and angled towards the capture geometry. Validation of sample capture was completed using a fluorescence microscope for visual verification. If the spheroid was not in the capture geometry but further up in the channel, tilting the device to 90˚ with respect to the ground and tapping the device against a surface often facilitated the spheroid to fall into the capture geometry.

After validating capture, the inlet and outlet were connected to a syringe pump and placed in a confocal for long term imaging. The confocal was also used to re-validate capture before testing. Figure 10 shows a 200µm diameter spheroid being captured by the geometry. Tumor fragments were used to validate the capture efficiency as well and provided similar results to the spheroids with the exception of oversized fragments which could not fit into the channel.

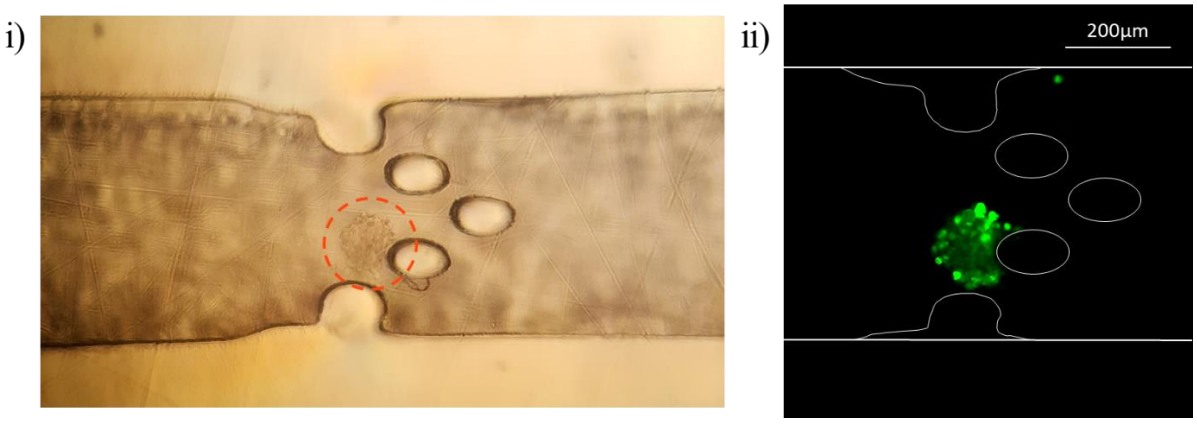

Figure 10. Visualization of a capture geometry evaluation using a 200µm CT26 spheroid. i): Brightfield image of captured 200µm diameter CT26 spheroid highlighted via a dotted red circle; ii): fluorescence image of the same spheroid with channel geometry overlay.

4.5 Evaluation of Fluidic Properties

Fluidic properties such as shear stress and localized velocity are important to evaluate with respect to the capture region of the device. The capture region is directly responsible for housing the biological sample in the center of the flow to promote perfusion of nutrients and the desired treatment for testing. However, the sample's location in the center of the channel can also impede flow thus exposing the sample to possibly harmful levels of shear stress and localized fluid velocity. Healthy levels of shear stress should not exceed 0.04Pa [3, 4, 23]. Shear rates above this threshold have been shown to be detrimental to cell health over time and could possibly break apart a spheroid. To ensure prevention of these detrimental levels of shear stress, the capture region was modeled in COMSOL 5.3 Multiphysics (COMSOL, Inc., 100 District Avenue Burlington, MA, USA). Figure 11 shows the 2D evaluations of the flow characteristics of the capture region with a captured 300µm diameter spheroid.

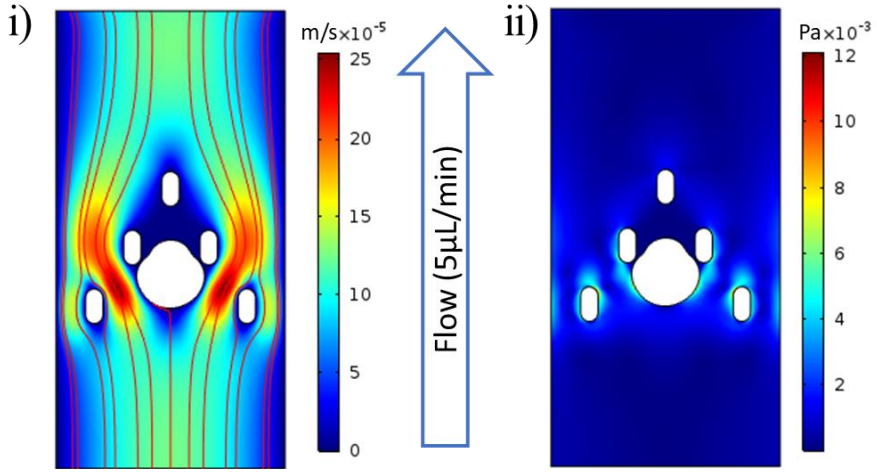

Figure 11. COMSOL models evaluating fluidic properties around the device's capture geometry. i): 2D colorized analysis of velocity intensity with streamlines; ii): 2D colorized analysis of shear stress depicting healthy levels of shear around the spheroid at 5µL/min.

The model was created by first designing a top down snapshot of the capture region with a 300µm diameter spheroid in SolidWorks 2016. A 300µm diameter spheroid was chosen as an

intermediate size since larger spheroids have restrictions to diffusion and smaller spheroids are not reliably captured. The worst-case scenario was modeled where the spheroid would obstruct as much of the channel as reasonably possible. The completed model was then imported into COMSOL where the 3D CAD model was sliced along the length of the channel to produce a 2D representation of the top down snapshot. A laminar flow model was used in conjunction with water as the medium at a flow rate of 5μL/min. Values for water were used instead of complete medium for simplicity with the knowledge that at such a low flow rates there would be little difference. The outputs of this simulation displayed healthy values of velocity intensity and shear stress surrounding the spheroid in the channel. Specifically, values of $6x10^{-3}$ Pa for shear stress and $2x10^{-5}$ m/s for velocity intensity are well below the threshold of 0.04Pa for healthy perfusion conditions. Further simulations can be seen in Appendix A.

4.6 Extended Viability Test

An important metric for assessment of the device's feasibility as a testing platform is its ability to sustain cell viability over an extended period of time, especially in comparison to the traditional method utilizing static culture techniques. Flow allows for more effective perfusion of nutrients into the biological sample in comparison to static culture, thus slowing the rate of cell death at the center of the sample. Additionally, flow acts as physiologically relevant stimuli which prompts *in vivo* like characteristics in the samples [2, 4].

In order to verify these claims, five devices were loaded with CT26 spheroids for comparison between flow and static culture conditions. Each sample was monitored via confocal microscopy over the course of 72 hours for cell death which was visualized via the use of APC Annexin V stain (ThermoFisher Scientific, Waltham, MA, USA) integrated into the media.

4.6.1 Imaging and Test Setup

A total of five CT26 spheroids were set up for imaging over a course of 3 days. Controls for this test consisted of a spheroid in a device without flow to evaluate the rate of cell death caused by the device. The loaded devices were placed in a Zeiss LSM 710 confocal microscope with temperature controls set to 37˚C with 5% CO2 for the duration of testing. Each device was connected side by side to ensure the platform was able to move to visualize each capture region. A schematic of the complete setup can be seen in Figure 12.

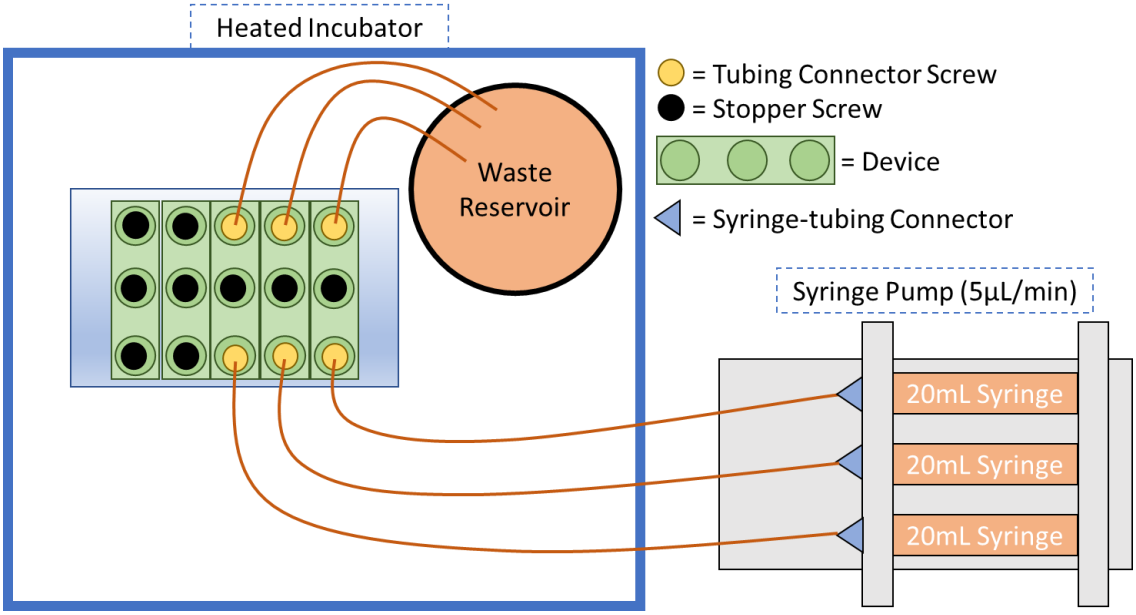

Figure 12. Schematic of test setup with a key to define crucial components.

A Harvard Apparatus syringe pump was chosen to provide flow since 20mL of media per device proved to be sufficient for the duration of the test. All device components were kept in their autoclave bags until needed to ensure sterility. Once the confocal was set up, positions were set for each capture region on a 10X lens with 14 imaging slices being chosen for each spheroid. Overall, 14 pictures were taken per sample every 10 hours.

4.6.2 Image Analysis

Analysis of each set of images was done via the use of ImageJ (NIH). As previously mentioned, the major metric for analysis was the decrease of fluorescence over the course of testing so each image was analyzed using the mean grey values and integrated density functionalities. These values along with area of the outlined spheroid were used to calculate the corrected total cell fluorescence (CTCF).

$$CTCF = Integrated\ Density - (Area\ of\ selected\ cell \times Mean\ fluorescence\ of\ background\ readings)$$

CTCF is used as a means of assessing brightness of fluorescence and was used to calculate the percent decrease in brightness when compared between the values at 10 hours and 70 hours [25]. 10 hours was chosen due to imaging issues with the 0 hour images. Each image was opened in ImageJ, the scale was set, and the outline of the spheroid was manually traced using an outlining tool. Each outline was done to capture the regions which were visually fluorescent resulting in minor differences in total area between each image. In addition to the outline of the spheroid, a second small circular section to the bottom left of each sample was analyzed to acquire the mean fluorescence of the background.

4.6.3 Viability Test Results

Images collected from the confocal were inspected individually for abnormalities and compounded to form the representative images seen in Figure 13 and 14. Both figures show the progression of cell death over the course of 3 days via seven 10-hour increments. Cell death is visualized by the decrease in intensity in CellTracker Green and the appearance of red fluorescence from cells undergoing apoptosis highlighted by APC Annexin V for the spheroid experiencing flow.

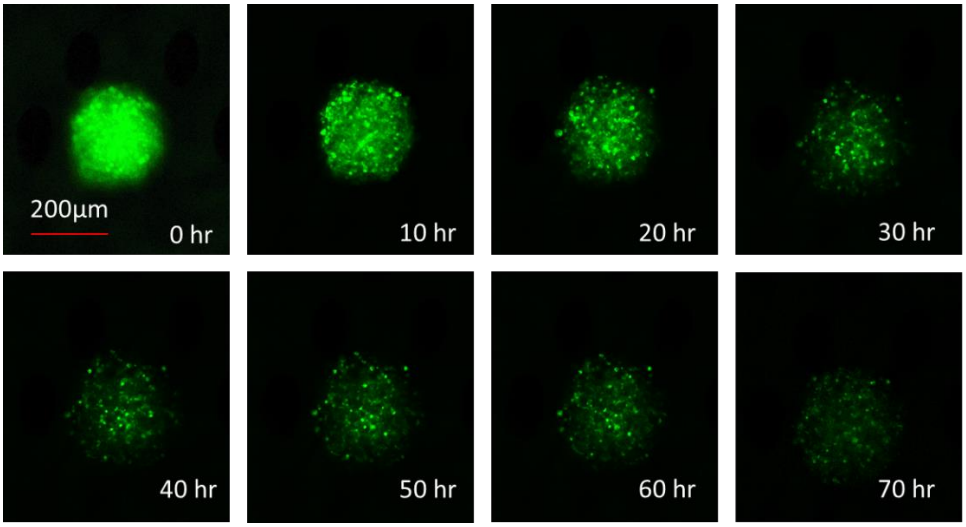

Figure 13. 300µm diameter CT26 spheroid in a device without flow decreasing in fluorescent intensity due to cell death over 70 hours.

Figure 13 depicts the progression of a control which was kept in a device with media containing APC Annexin V without flow. Over the course of 3 days the intensity of CellTracker Green greatly decreased by over 74% and the structure of the spheroid began to degrade. This degradation is most noticeable starting at around 50 hours where the spheroid reduces minorly in diameter. Both of these are indications of significant death over the course of the 3 days which was expected. The Annexin V within the media, however, never effectively diffused to the spheroid.

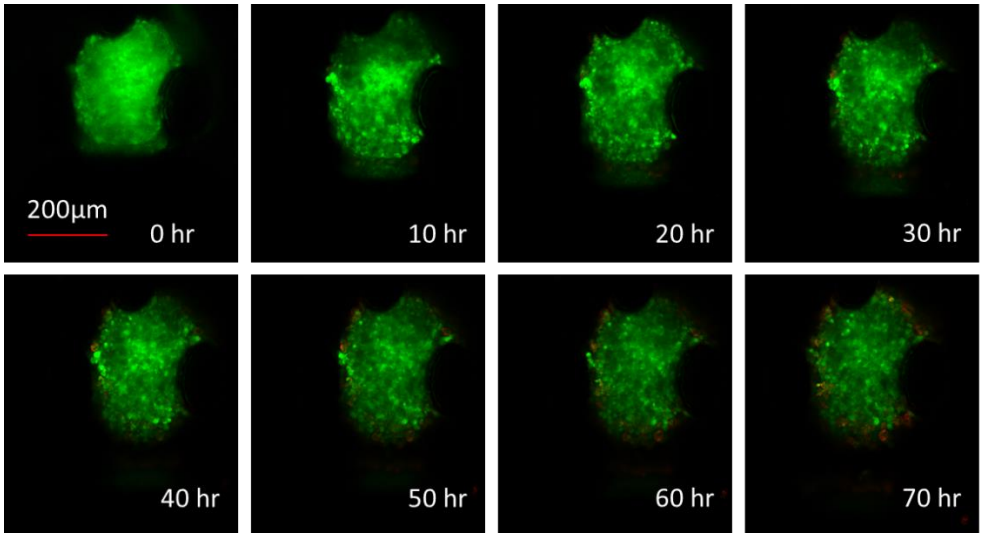

Figure 14. 300µm diameter CT26 spheroid in a device with flow decreasing in fluorescent intensity due to cell death over 70 hours.

Comparatively, Figure 14 shows a spheroid trapped with constant perfusion of Annexin V infused media allowing for effective diffusion into the cells. The CellTracker Green decreases in intensity over the course of 3 days by only 28% suggesting flow increased the longevity of the spheroid. Around hour 10, some red can be seen on the bottom of the spheroid which is the side directly encountering the flow first. By the 30th hour the Annexin V stain was appearing on the opposite side of the spheroid which was further validated by the final image which has red all around the perimeter of the spheroid. The spheroid held in Figure 14 was captured by three posts at the center of the channel which is depicted in Appendix Figure A1 for clarity. It should be noted that the regions of the spheroid in direct contact with the posts did not show a disproportionate amount cell death compared to the rest of the spheroid. However, due to the contact with the posts, Annexin V did not stain those regions.

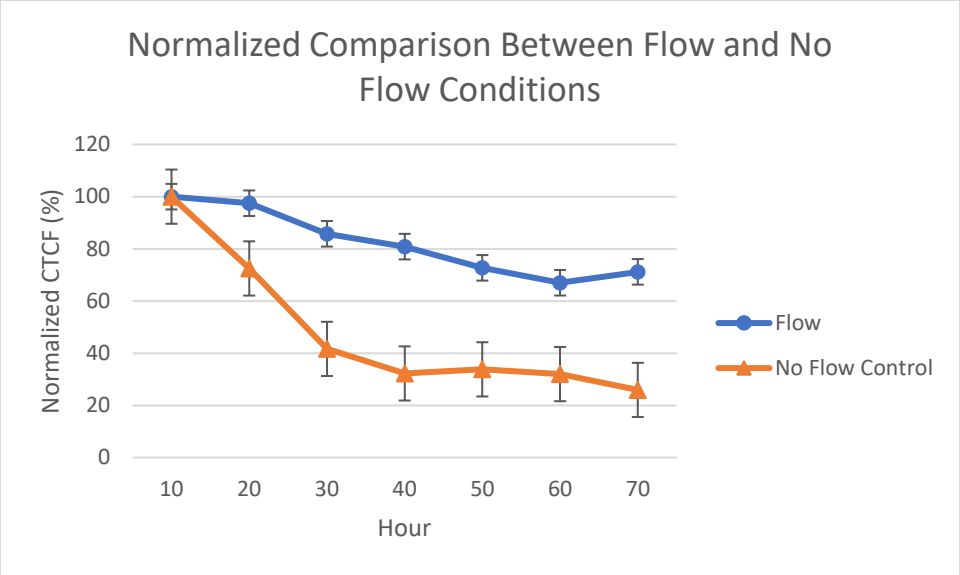

Figure 15. Graph depicting the large difference between the normalized CTCF values associated with the flow and no flow control over the course of 70 hours.

Overall, Figure 15 shows the normalized CTCF values between the control and the flow condition. The graph is normalized with respect to hour 10 instead of hour 0 since all of the automated hour 0 pictures were extremely dim compared to what they actually were at the time. Therefore, the 0 hour images seen in Figure 13 and 14 have been artificially brightened post imaging to better represent their original brightness. This, however, excludes them from use in image analysis.

The goal of this test was to use both the decrease in CellTracker Green fluorescence over time via CTCF and the appearance of APC Annexin V due to apoptosis as metrics for determining cell death between the flow and static conditions. While CTCF was effective at analyzing CellTracker Green decrease in fluorescence over time, the lack of visible APC Annexin V staining in the control prevents the conclusion of extended viability over time. Furthermore, the decrease in fluorescence over time can also be attributed to cell proliferation which can dilute out CellTracker Green. Overall, CTCF alone cannot conclusively validate extended viability although it can act as a supportive measurement for future studies.

5 Conclusion

The device I developed and evaluated in this thesis is capable of capturing biological samples with the potential of extending their viability compared to traditional methods for cancer therapeutic studies. Additionally, the manufacturing time and scalability of my device surpasses that of traditional platforms and modern variations such as TAP and EVIDENT via the use of commercial 3D printing technology in conjunction with novel microfluidics. Specifically, the device can be produced and ready for use in an hour in a half compared to the multiweek to month time frame for traditional microfluidic platforms. The optimized 3D printing parameters and minimalistic design allow for rapid iterations to adapt to various sample sizes while maintaining device integrity and flexibility for testing configuration.

The Asiga MAX X27 in conjunction with the biocompatible Pro3dure GR1 resin proved to be an effective and unique combination for device creation. The 3D printing platform was optimized via the use of a custom resolution testing platform to reach the extremely small features required for the final device with only 2.1% (9.2±8.2μm) and 2.9% (22±10μm) variances in height and width respectively. Furthermore, a series of protocols were created regarding post printing treatments to improve the imaging clarity and strength of the device all while keeping production time under two hours. The resulting device is 46mm by 16mm by 10.6mm while still integrating all critical components such as a threaded inlet and outlet, bubble trap, and specialized sample capture geometry.

Using a combination of CT26 spheroids and human tumor fragments, the device's capture efficiency was assessed and proved to safely and reliably capture samples larger than 200μm in diameter. COMSOL modeling was used to validate that once a spheroid was captured, it was being exposed to healthy levels of velocity intensity and shear stress. Finally, the device's

ability to prolong cell life was evaluated via CT26 spheroids over the course of three days where the device exceeded the CTCF values of the static flow control by close to 50%. Although, this metric alone cannot validate extended viability without a second live dead stain.

These tests along with the simplistic design and low production time position this platform as an attractive medium to supplant current drug testing platforms. This fact is especially relevant with regard to immunotherapy based testing as static culture devices cannot match the *in vivo* like immune reactions of the device discussed in this report. Compared to its competition, this microfluidic device is the first of its kind to capture tumor spheroids in an array of micro posts created solely via 3D printing. Ultimately, this device will enable researchers and clinicians alike to test various immunotherapies in a scalable, rapid, and *in vivo* relevant manner.

6 Future Work

The work described in this thesis has built a foundation which can be expanded on in a variety of ways to further validate the device's benefits as a cellular testing platform. Most importantly out of these options is the use of immunology treatments with the device. One of the driving reasons for creation of this platform was to provide the field of immuno-oncology with a platform to evaluate immunology therapies with *in vivo* like conditions including flow, cell-cell interactions, and immune cell-tumor cell interactions. The use of CT26 cells help pave the way for future immune based testing using combination treatments such as TIL and anti PD-1. Going forward, tests like those previously mentioned can help validate the device as an effective *in vitro* platform in conjunction with established mouse models such as MC38 and B16F10 [2, 24]. Live dead cell assays as well as spheroid deformation would also be used as additional metrics of viability. Eventually this device could be used in clinics to provide patients with rapid feedback on which immunotherapy best works against their cancer using a tumor biopsy.

One area which affects the device's production time is the exploration of other ways to improve the imaging quality of the device. Currently, as mentioned in section 4.1, the devices require multiple rounds of polishing to reach acceptable clarity. To circumvent the multiple rounds of polishing a finer level of sand paper such as 1µm grit sandpaper or printing on to a glass slide could be explored. In addition to this, further design optimization between the Asiga MAX X27 and the device to increase feature resolution of the capture geometry would be beneficial. Smaller feature resolution would allow for samples below 200µm to be captured more reliably.

Exploring other types of biological samples such as organoids would also further validate the flexibility of the device. Organoids are multicellular in composition and match *in vivo*

constructs much more than spheroids at the price of size control of the organoid. With the ease of iteration and production associated with the device, devices could be custom made to match each organoid sample. The combination of organoids and flow-based interactions with immune cells or drugs is largely unexplored and could produce new novel research options for the future. Additionally, further analysis on the biological sample could be done post exposure to the desired treatment by collecting the biological sample from the device post testing. Secondary viability tests could be performed as well as genomic assessments and assays to evaluate the effectiveness of the cancer treatment.

References

[1] K. W. Oh, "Multidisciplinary Role of Microfluidics for Biomedical and Diagnostic Applications: Biomedical Microfluidic Devices," *Micromachines,* vol. 8, *(12),* pp. 343, 2017. Available: https://www.ncbi.nlm.nih.gov/pubmed/30400533. DOI: 10.3390/mi8120343.

[2] N. Moore *et al*, "A multiplexed microfluidic system for evaluation of dynamics of immune-tumor interactions," *Lab on a Chip,* vol. 18, *(13),* pp. 1844-1858, 2018. Available: https://search.proquest.com/docview/2045272947. DOI: 10.1039/c8lc00256h.

[3] A. L. Beckwith, J. T. Borenstein and L. F. Velasquez-Garcia, "Monolithic, 3D-Printed Microfluidic Platform for Recapitulation of Dynamic Tumor Microenvironments," *Jmems,* vol. 27, *(6),* pp. 1009-1022, 2018. Available: https://ieeexplore.ieee.org/document/8492355. DOI: 10.1109/JMEMS.2018.2869327.

[4] A. B. Holton *et al*, "Microfluidic Biopsy Trapping Device for the Real-Time Monitoring of Tumor Microenvironment," *PloS One,* vol. 12, *(1),* pp. e0169797, 2017. Available: https://www.ncbi.nlm.nih.gov/pubmed/28085924. DOI: 10.1371/journal.pone.0169797.

[5] M. E. Dolega *et al*, "Cell-like pressure sensors reveal increase of mechanical stress towards the core of multicellular spheroids under compression," *Nature Communications,* vol. 8, *(1),* pp. 14056, 2017. Available: https://www.ncbi.nlm.nih.gov/pubmed/28128198. DOI: 10.1038/ncomms14056.

[6] (). *Leading Cancer Cases and Deaths, Male and Female, 2016.* Available: https://gis.cdc.gov/Cancer/USCS/DataViz.html.

[7] H. Phuengkham *et al*, "Nanoengineered Immune Niches for Reprogramming the Immunosuppressive Tumor Microenvironment and Enhancing Cancer

Immunotherapy," *Advanced Materials,* vol. 31, *(34),* pp. e1803322-n/a, 2019. Available: https://onlinelibrary.wiley.com/doi/abs/10.1002/adma.201803322. DOI: 10.1002/adma.201803322.

[8] N. Convery and N. Gadegaard, "30 years of microfluidics," *Micro and Nano Engineering,* vol. 2, pp. 76-91, 2019. Available: https://www.openaire.eu/search/publication?articleId=doajarticles::84b10b4462b4102925df96bf16bdd8e5. DOI: 10.1016/j.mne.2019.01.003.

[9] H. Nguyen *et al,* "Low-Cost, Accessible Fabrication Methods for Microfluidics Research in Low-Resource Settings," *Micromachines,* vol. 9, *(9),* pp. 461, 2018. Available: https://www.ncbi.nlm.nih.gov/pubmed/30424394. DOI: 10.3390/mi9090461.

[10] J. C. McDonald *et al,* "Fabrication of microfluidic systems in poly(dimethylsiloxane)," *Electrophoresis,* vol. 21, *(1),* pp. 27-40, 2000. Available: https://onlinelibrary.wiley.com/doi/abs/10.1002/(SICI)1522-2683(20000101)21:1<27::AID-ELPS27>3.0.CO;2-C. DOI: 10.1002/(SICI)1522-2683(20000101)21:1<27::AID-ELPS27>3.0.CO;2-C.

[11] D. J. Beebe, G. A. Mensing and G. M. Walker, "PHYSICS AND APPLICATIONS OF MICROFLUIDICS IN BIOLOGY," *Annual Review of Biomedical Engineering,* vol. 4, *(1),* pp. 261-286, 2002. Available: https://www.ncbi.nlm.nih.gov/pubmed/12117759. DOI: 10.1146/annurev.bioeng.4.112601.125916.

[12] D. S. Kim *et al,* "Disposable integrated microfluidic biochip for blood typing by plastic microinjection moulding," *Lab on a Chip,* vol. 6, *(6),* pp. 794, 2006. Available: https://www.ncbi.nlm.nih.gov/pubmed/16738733. DOI: 10.1039/b516495h.

[13] N. Bhattacharjee *et al*, "The upcoming 3D-printing revolution in microfluidics," *Lab on a Chip*, vol. 16, *(1)*, pp. 172-1742, 2016.
Available: https://search.proquest.com/docview/1788223879. DOI: 10.1039/c6lc00163g.

[14] A. Kulasinghe *et al*, "The Use of Microfluidic Technology for Cancer Applications and Liquid Biopsy," *Micromachines*, vol. 9, *(8)*, pp. 397, 2018.
Available: https://www.ncbi.nlm.nih.gov/pubmed/30424330. DOI: 10.3390/mi9080397.

[15] (October 3,). *Precision Medicine in Cancer Treatment*.
Available: https://www.cancer.gov/about-cancer/treatment/types/precision-medicine.

[16] F. Hirschhaeuser *et al*, "Multicellular tumor spheroids: An underestimated tool is catching up again," *Journal of Biotechnology*, vol. 148, *(1)*, pp. 3-15, 2010.
Available: http://dx.doi.org/10.1016/j.jbiotec.2010.01.012. DOI: 10.1016/j.jbiotec.2010.01.012.

[17] R. Foty, "A Simple Hanging Drop Cell Culture Protocol for Generation of 3D Spheroids," *Journal of Visualized Experiments*, 2011.

[18] R. Ebner *et al*, "Spheroid-based drug screen: considerations and practical approach," *Nature Protocols*, vol. 4, *(3)*, pp. 309-324, 2009. Available: http://dx.doi.org/10.1038/nprot.2008.226. DOI: 10.1038/nprot.2008.226.

[19] (). *Casting, Equilibrating and Seeding the 3D Petri Dish*.
Available: https://www.microtissues.com/protocols.

[20] N. K. Finnberg *et al*, "Application of 3D tumoroid systems to define immune and cytotoxic therapeutic responses based on tumoroid and tissue slice culture molecular signatures," *Oncotarget*, vol. 8, *(40)*, pp. 66747-66757, 2017.
Available: https://www.ncbi.nlm.nih.gov/pubmed/28977993. DOI: 10.18632/oncotarget.19965.

[21] H. Fan, U. Demirci and P. Chen, "Emerging organoid models: leaping forward in cancer research," *Journal of Hematology & Oncology*, vol. 12, *(1)*, pp. 1-142, 2019. Available: https://search.proquest.com/docview/2340763715. DOI: 10.1186/s13045-019-0832-4.

[22] D. Hanahan and R. Weinberg, "Hallmarks of Cancer: The Next Generation," *Cell*, vol. 144, *(5)*, pp. 646-674, 2011. Available: http://dx.doi.org/10.1016/j.cell.2011.02.013. DOI: 10.1016/j.cell.2011.02.013.

[23] Y. Kawai *et al*, "Pivotal roles of shear stress in the microenvironmental changes that occur within sentinel lymph nodes," *Cancer Science*, vol. 103, *(7)*, pp. 1245-1252, 2012. Available: https://onlinelibrary.wiley.com/doi/abs/10.1111/j.1349-7006.2012.02289.x. DOI: 10.1111/j.1349-7006.2012.02289.x.

[24] R. W. Jenkins *et al*, "Ex Vivo Profiling of PD-1 Blockade Using Organotypic Tumor Spheroids," *Cancer Discovery*, vol. 8, *(2)*, pp. 196-215, 2018. Available: https://www.ncbi.nlm.nih.gov/pubmed/29101162. DOI: 10.1158/2159-8290.CD-17-0833.

[25] (). *Counting of Total Fluorescence in a Cell*. Available: https://vlab.amrita.edu/?sub=3&brch=278&sim=1474&cnt=1.

Appendix A Figures

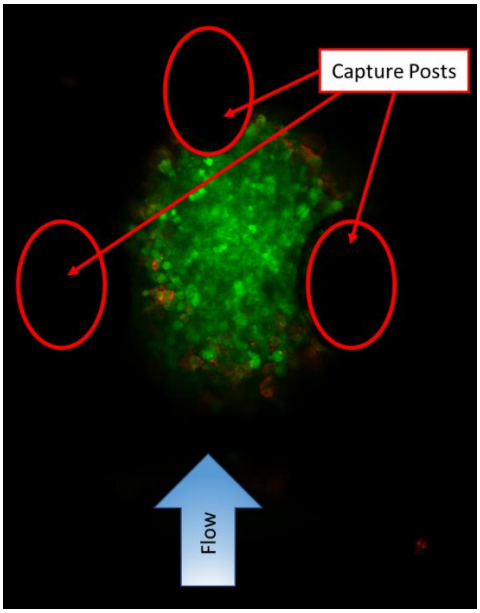

Figure A1. Positioning of the CT26 spheroid with respect to the capture posts and direction of flow.

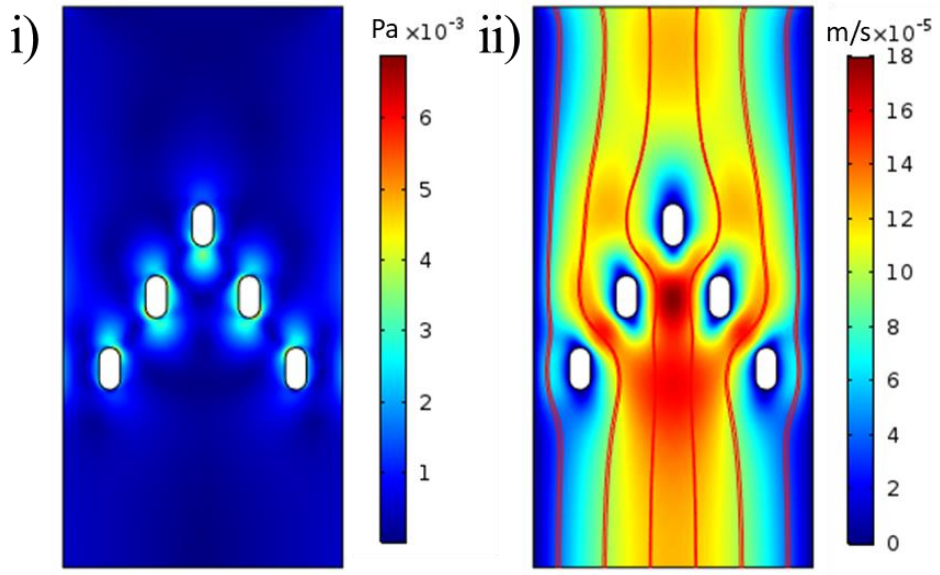

Figure A2. COMSOL models evaluating fluidic properties around the device's capture geometry without a spheroid. i): 2D colorized analysis of shear stress depicting healthy levels of shear around the spheroid at 5µL/min; ii): 2D colorized analysis of velocity intensity with streamlines.

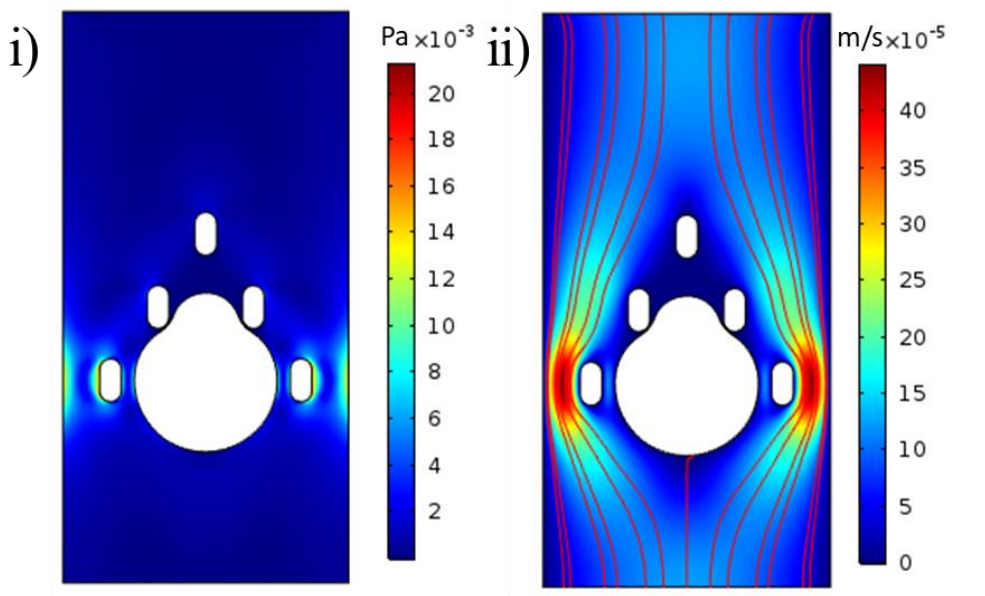

Figure A3. COMSOL models evaluating fluidic properties around the device's capture geometry with a 500µm diameter spheroid. i): 2D colorized analysis of shear stress depicting healthy levels of shear around the spheroid at 5µL/min; ii): 2D colorized analysis of velocity intensity with streamlines.

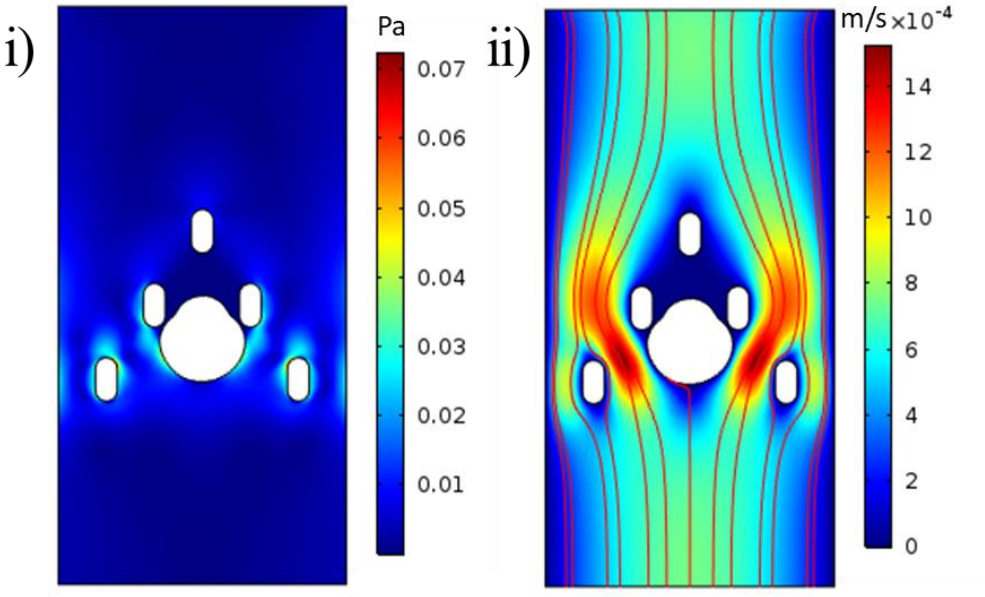

Figure A4. COMSOL models evaluating fluidic properties around the device's capture geometry with a 300µm diameter spheroid. The flow rate was increased until the healthy threshold of 0.04Pa was observed at 30µL/min i): 2D colorized analysis of shear stress depicting healthy levels of shear around the spheroid at 30µL/min; ii): 2D colorized analysis of velocity intensity with streamlines.

Appendix B Tables

Table B1. All factors tested, associated results from the Resolution Testing Device normalized with respect to the CAD file, and device information outlining the CAD file parameters. There were 5 revisions of this testing platform, each with a different combination of number of posts and channels. The best results are colored green to simplify evaluation. A Layer Thickness of 0.05, a Multiplier of 1, and an offset value of 0.272 provided the best results overall.

Factor Combinations Tested			Resolution Testing Device Results									Device Information			
Slice Thickness	Cure Through Multiplier	Offset Value	Pillars (0.25mm) Developed	Pillars (0.125mm) Developed	Open Channels	Clear Channels	Topless Channels	Blocked Channels	.25mm pillar (%)	.125 pillar (%)	channel (%)	Device Rev	Device #	Ch #	Post #
0.01	1	0.1	5	5	3	3	0	1	50	50	75	3	7	4	10
0.01	1	0.01	0	4	1	0	0	3	0	40	0	3	16	4	10
0.025	1	0.1	0	0	0	0	0	4	0	0	0	1	3	4	8
0.05	1	0.1	0	0	0	0	0	4	0	0	0	0	1	4	6
0.05	1	0.2	8	8	3	2	1	1	80	80	40	4	20	5	10
0.05	1	0.272	8	8	6	5	1	0	80	80	83.3	5	27	6	10
0.05	0.5	0.272	8	8	3	3	1	2	80	80	60	4	22	5	10
0.05	2	0.272	9	9	0	0	5	0	90	90	0	4	23	5	10
0.05	0.1	0.272	8	8	3	3	1	2	80	80	60	4	24	5	10
0.1	1	0.1	7	8	3	1	0	1	70	80	25	3	17	4	10
0.1	1	0.04	6	7	3	1	0	1	60	70	25	3	14	4	10
0.1	1	0.6	9	9	0	0	4	0	90	90	0	3	11	4	10
0.1	1	0.06	7	8	3	2	0	1	70	80	50	3	12	4	10
0.1	1	0.01	6	7	3	1	0	1	60	70	25	3	15	4	10
0.1	1	0.2	8	8	3	3	1	2	80	80	60	4	19	5	10

Appendix C Protocols

C1 Polishing Procedure

Date of Creation: 1/22/2020

Author: Alex Markoski

Last modified by and when: Alex Markoski 4/3/2020

1. 1 min of circular motion using 3,600 Micro Mesh (8 um)
2. Isopropanol and cotton swab to clean the area
3. 1 min of circular motion using 4,000 Micro Mesh (5 um)
4. Isopropanol and cotton swab to clean the area
5. 1 min of circular motion using 6,000 Micro Mesh (4 um)
6. Isopropanol and cotton swab to clean the area
7. Repeat 1-6 skipping 3&4
8. Based off profilometer analysis determine if further repetitions are required

White Aluminum Oxide

1. Place small dollop of Al_2O_3 on a kimwipe
2. Create a ball of kipwipes to smear the dollop until a residue is left on the ball
3. Dab the ball on to the surface of device and use a circular motion to polish
4. Clean thoroughly with Isopropanol and cotton swab to clean the area

C2 Protocol For 3D Printing and Post Treatment

Date of Creation: 1/22/2020

Author: Alex Markoski

Last modified by and when: Alex Markoski 1/23/2020

Preparation:

1. Acquire paper towels, gloves, and glasses
2. Assess the amount of resin in the resin bath (should be 10mm height)
3. Start up the 3D printer if it is off by pressing the button on the top of the 3D printer
4. Go to the LED menu (controls-->LED)
5. Turn on the LED for ~10 seconds to produce a cured rectangle for removal of remnants from previous builds
6. Remove the cured rectangle from the bath via the thin metal remover
    a. Hold the rectangle over the corner of the bath until a majority of the uncured resin drips back into the bath
7. Throw away the cured rectangle, clean the thin metal remover, and get new gloves

3D Printing:

1. Create desired build in SolidWorks
2. Save as a STL file
3. Open the Asiga Composer and rotate the build and then autoplace the build
4. Connect the laptop to the 3D printer via the red ethernet cable
5. Save the Asiga Composer file and send the build to the printer
    a. If the program doesn't find the 3D printer try to close the program and open again

6. On the 3D printer select the printing option from the starting screen and choose the “next build” option
    a. Once the build has been found on the 3D printer the ethernet cable can be detached from the laptop
7. Confirm the material and start the build if…
    a. There aren’t any bubbles or contaminants in the bath

Post Process:

Removal and Cleaning

1. Using new gloves, glasses, and the thin metal remover scrape the new build from the building platform
    a. Place the thin metal remover on to the edge of the building platform at a ~25 degree angle
    b. Push the remover across the building platform lightly as to not scratch the building platform but with enough contact to find the build
    c. Once the build is found apply force gradually while holding an open hand underneath the platform to catch the build once it is removed
2. Take the build and place it in the dirty >97% iso container and gradually flip the container over till the build is submerged
3. Manually mix the solution for 3-5 min
4. Using tweezers remove the build from the dirty container and place it into the clean >97% iso container and repeat step 3
5. Remove the build via tweezers and place it onto a paper towel and dab the build to dry it.

6. For devices with internal channels (ex CD series of devices) connect tubing to the inlet and outlet and place stopper in the bubble trap.
7. Fill a 3mL syringe with 100% isopropanol with a 1mm tip and connect it to the outlet side.
8. Open the clean >97% iso container and place the inlet tubing in it.
9. Flow ~1.5mL through the device then pause and remove the bubble trap stopper and flow the remaining ~1.5mL through the device.
10. Remove the syringe from the connected 1mm tip and fill with air and then reconnect to the system.
11. Forcibly push air through the device until a majority of iso is removed.
12. Use a high-power air gun to remove the rest of the iso from the channel.
13. Check the channel to make sure that the channel is clean of any visible remnants, if not repeat steps 9 through 12 until clean.
14. Label the device with the proper ID.

Polishing

See polishing protocol.

Curing

1. Turn on N2 gas slowly with the door of the oven open and stop turning when you hear the hissing.
2. Place the build in the center of the oven and close the door.
3. Wait 30 seconds to let the N2 fill the chamber.

4. Turn on the power of the oven and input 3 minutes into the timer (displayed as 3.0).
5. Start the oven.
6. After 3 minutes remove the build and turn off the N2.
7. Turn off the power for the oven.